CONFIDENTIAL

Master of Science Thesis

Process water treatment using eutectic freeze crystallization for the HyVent Metal Recovery Process from Spent Hydrotreating Catalysts

Conceptual process design of the salt sludge separation

Berend Nootenboom

November 30, 2016

Mechanical Engineering

Delft University of Technology

MSCCONFIDENTIAL

Process water treatment using eutectic freeze crystallization for the HyVent Metal Recovery Process from Spent Hydrotreating Catalysts

Conceptual process design of the salt sludge separation

MASTER OF SCIENCE THESIS

For the degree of Master of Science in Mechanical Engineering:
Sustainable Process and Energy Technology at Delft University of Technology

Berend Nootenboom

November *30*, 2016

Faculty of Mechanical, Maritime and Materials Engineering (3mE) · Delft University of Technology

EFC
separations

HyVent
Technology

TU Delft
Delft
University of
Technology

Copyright © Delft University of Technology
All rights reserved.

DELFT UNIVERSITY OF TECHNOLOGY
DEPARTMENT OF
PROCESS AND ENERGY

The undersigned hereby certify that they have read and recommend to the Faculty of Mechanical, Maritime and Materials Engineering (3mE) for acceptance a thesis entitled

PROCESS WATER TREATMENT USING EUTECTIC FREEZE CRYSTALLIZATION FOR THE HYVENT METAL RECOVERY PROCESS FROM SPENT HYDROTREATING CATALYSTS

by

BEREND NOOTENBOOM

in partial fulfillment of the requirements for the degree of

MASTER OF SCIENCE MECHANICAL ENGINEERING: SUSTAINABLE PROCESS AND ENERGY TECHNOLOGY

Dated: November 30, 2016

Supervisor(s):

Dr.ir. H.J.M. Kramer

Dr. J. van Spronsen

Reader(s):

Prof.dr.ir. A.I. Stankiewicz

Dr. ir. C.A. Infante Ferreira

Table of Contents

1 Introduction **1**

1-1 Research objective: A new concept for separation of salt sludge produced by the HyVent metal recovery process . . . 2

1-2 Structure of the thesis . . . 5

2 Eutectic freeze Crystallization **7**

2-1 Crystallization . . . 7

2-1-1 Supersaturation . . . 8

2-1-2 Nucleation . . . 9

2-1-3 Crystal growth . . . 13

2-1-4 Crystallization methods . . . 14

2-2 Separation principle of eutectic freeze crystallization . . . 16

2-3 EFC process for ternary systems . . . 17

2-4 State of the art of EFC . . . 19

3 EFC batch experiments **23**

3-1 Experimental setup for the EFC batch experiments . . . 25

3-2 Batch experiments with aqueous solutions of sodium sulfate and sodium nitrate 26

3-2-1 Solubility data and phase diagram of the sodium system . . . 26

3-2-2 Experimental procedure and solution compositions . . . 28

3-2-3 Results and discussion . . . 30

3-3 Batch experiments with aqueous solutions of potassium sulfate and potassium nitrate . . . 34

3-3-1 Solubility data and phase diagram of the potassium system . . . 34

3-3-2 Experimental procedure and solution compositions 35
3-3-3 Results and discussion 36
3-4 Conclusions 40
3-4-1 Implications for the process design 41

4 Removal of molybdate and vanadate as precipitates of calcium 43
4-1 Experimental setup for the calcium precipitation batch experiments 45
4-2 Experimental procedure 45
4-2-1 Effect of calcium dosage and pH 45
4-2-2 Effect of residence time 47
4-3 Results and discussion 47
4-3-1 Mean particle size 49
4-4 Conclusions 51
4-4-1 Implications for the process design 51

5 Process flow model for the Salt Sludge Separation process 53
5-1 Development of process model 54
5-1-1 Assumptions 54
5-1-2 Model decomposition and input parameters 55
5-1-3 Operating region of the EFC crystallizer 56
5-1-4 Mass balance equations 58
5-1-5 Energy balance equations 65
5-2 Dimensioning of equipment and fixed costs 69
5-2-1 EFC crystallizer and cooling machine 69
5-2-2 Buffer vessel 70
5-2-3 Precipitation vessel 71
5-2-4 Design of settling device 71
5-2-5 Vacuum belt filters 73
5-3 Energy and raw material consumption and variable costs 74
5-4 Product flow and revenue 74
5-5 OPEX and Pay Back time of the process 75

6 Model results and optimization of the process 77
6-1 Model results 78
6-2 Options for optimization 82
6-3 Possibilities for heat integration 83
6-3-1 Comparison of results 85

7 Case studies and Final process design 89
7-1 Case study 2: Cooling crystallization and EFC in separate crystallizers 89
7-2 Case study 3: Two EFC crystallizers connected in series 90
7-3 Case study results and Final process design 91
7-4 Case 4: Discharge the brine, no process and no treatment 94

8 Conclusions and Recommendations 97
8-1 Conclusions 97
8-2 Recommendations 99

List of Figures

1-1 Block diagram representing and the salt sludge separation process 3
1-2 Black box process with specified input stream and desired output. 4
1-3 Schematic overview of the thesis 6

2-1 Basic phase diagram of a binary system. 8
2-2 Gibbs free energy diagram for homogeneous nucleation showing the critical nucleus radius. [14] 11
2-3 Effect of supersaturation on the homogeneous and heterogeneous nucleation rates. [13] 11
2-4 Basic phase diagram of a binary system in which the metastable zone limited is shown as the red line parallel to the black solubility curve. Furthermore, the crystallization path of a typical cooling crystallization process is shown. . 13
2-5 Typical phase diagram of an inorganic aqueous solution. 16
2-6 Schematic representation of the EFC process 17
2-7 Ternary phase diagram of a sodium bicarbonate - sodium carbonate - water system 19
2-8 Schematic representation of a cooled disk column crystallizer. 20
2-9 Cross sectional top view of the scraped cooled wall crystallizer. 20
2-10 Scaled up version of the cooled disk column crystallizer. 21
2-11 Cross sectional top view of the scraped cooled wall crystallizer. 21
2-12 Heat exchanger module of the scaled up scraped cooled wall crystallizer. . . . 21

3-1 Option 1: EFC process only. 24
3-2 Schematic representation of the experimental setup used in the batch experiments. 26

3-3 Ternary phase diagram of the Na_2SO_4, $NaNO_3$, H_2O system. The blue and orange lines resemble the eutectic lines of $Na_2SO_4 \cdot 10H_2O$ - H_2O and $NaNO_3$ - H_2O respectively. 27

3-4 Temperature profile of solution S1 with the time in hours on the x-axis and the temperature on the y-axis. The blue line represents the solution temperature, while the red line represents the coolant temperature. 30

3-5 Temperature profile of solution S2 with the time in hours on the x-axis and the temperature on the y-axis. The blue line represents the solution temperature, while the red line represents the coolant temperature. 30

3-6 Temperature profile of solution S3 with the time in hours on the x-axis and the temperature on the y-axis. The blue line represents the solution temperature, while the red line represents the coolant temperature. 30

3-7 Temperature profile of solution S4 with the time in hours on the x-axis and the temperature on the y-axis. The blue line represents the solution temperature, while the red line represents the coolant temperature. 30

3-8 Ternary phase diagram of the Na_2SO_4, $NaNO_3$, H_2O system, in which the experimentally obtained eutectic points (orange) are shown together with those from literature (blue). 30

3-9 Mean ice purity (in %) of solutions S1 to S4 plotted against the amount of washing of the crystals with subcooled water, ranging from unwashed to 5x washing. 32

3-10 On the left y-axis the mean ice purity (in %) of solutions SM and SMV1 and on the right y-axis the concentration (in ppm) of molybdate and vanadate, both plotted against the amount of washing of the crystals with subcooled water. 32

3-11 Mean sodium sulfate decahydrate salt composition from solutions S1 to S3. The salt composition (in w%) is plotted against the amount of washing of the crystals with a saturated solution of sodium sulfate, ranging from unwashed to 5x washing. 33

3-12 Sodium sulfate decahydrate salt composition from solution SS. The salt composition (in w%) is plotted against the amount of washing of the crystals with water, ranging from unwashed to 2x washing. 33

3-13 Salt composition from solution SM, The salt composition (in w%) is plotted against the amount of washing of the crystals with water. 33

3-14 Salt composition from solution SMV, The salt composition (in w%) is plotted against the amount of washing of the crystals with water. 33

3-15 Ternary phase diagram of the K_2SO_4, KNO_3, H_2O system. The blue and orange lines resemble the eutectic lines of K_2SO_4 - H_2O and KNO_3 - H_2O respectively. 35

3-16 Photo of the encountered scaling on the stirrer. The scale layer consists of mostly ice with potassium sulfate crystals. Similar scaling layers caused the beaker to break in other experiments with the potassium system. 36

3-17 Temperature profile of solution K1 with the time in hours on the x-axis and the temperature on the y-axis. The black line represents the solution temperature, while the red line represents the coolant temperature. 37

3-18 Temperature profile of solution K2 with the time in hours on the x-axis and the temperature on the y-axis. The black line represents the solution temperature, while the red line represents the coolant temperature. 37

3-19 Temperature profile of solution K4 with the time in hours on the x-axis and the temperature on the y-axis. The black line represents the solution temperature, while the red line represents the coolant temperature. 37

3-20 Temperature profile of solution K5 with the time in hours on the x-axis and the temperature on the y-axis. The black line represents the solution temperature, while the red line represents the coolant temperature. 37

3-21 Ternary phase diagram of the K_2SO_4, KNO_3, H_2O system, in which the experimentally obtained eutectic points (orange) are shown together with those from literature (blue). 38

3-22 Mean ice purity (in %) of solutions K1 to K5 plotted against the amount of washing of the crystals with subcooled water, ranging from unwashed to 5x washing. 38

3-23 On the left y-axis the mean ice purity (in %) of solutions KM and KMV and on the right y-axis the concentration (in ppm) of molybdate and vanadate, both plotted against the amount of washing of the crystals with subcooled water. 38

3-24 Mean potassium sulfate salt composition from solutions K2 and K3. The salt composition (in w%) is plotted against the amount of washing of the crystals with a saturated solution of potassium sulfate, ranging from unwashed to 5x washing. 39

3-25 Potassium sulfate salt composition from solutions KS. The salt composition (in w%) is plotted against the amount of washing of the crystals with water, ranging from unwashed to 2x washing. 39

3-26 Salt composition from solution KM, The salt composition (in w%) is plotted against the amount of washing of the crystals with water. 39

3-27 Salt composition from solution KMV, The salt composition (in w%) is plotted against the amount of washing of the crystals with water. 39

3-28 Block diagram of the process with the implemented results from the EFC batch experiments. 41

4-1 Block diagram representing the removal of molybdate and vanadate form the concentrated nitrate stream by the addition of calcium hydroxide. 44

4-2 Schematic representation of the experimental setup used in the calcium precipitation experiments. 45

4-3 Experiments CS1 and CS2: Concentration in ppm of molybdate, vanadate and calcium in the solution plotted against the pH of the solution. Also two different dosages of CaO were used: equimolar amount and double molar amount with respect to the molybdate and vanadate concentration of the solution. 47

4-4 Experiments CK1 and CK2: Concentration in ppm of molybdate, vanadate and calcium in the solution plotted against the pH of the solution. Also two different dosages of CaO were used: equimolar amount and double molar amount with respect to the molybdate and vanadate concentration of the solution. 48

4-5 Experiment CSV1: Concentration in ppm of molybdate, vanadate and calcium in the solution plotted against the pH of the solution. 48

4-6 Experiment CKV1: Concentration in ppm of molybdate, vanadate and calcium in the solution plotted against the pH of the solution. 48

4-7 Experiment CSV1: Composition in w% of the formed solid phase during the precipitation process 48

4-8 Experiment CKV1: Composition in w% of the formed solid phase during the precipitation process. For pH # and # insufficient solids had formed. 48

4-9 Experiment CSV2: Concentration in ppm of molybdate, vanadate and calcium in the solution plotted against the residence time. In this experiment the pH was not reduced by the addition of nitric acid. 49

4-10 Experiment CSV3: Concentration in ppm of molybdate, vanadate and calcium in the solution plotted against the residence time. In this experiment the pH was reduced to about # by the addition of nitric acid. 49

4-11 Experiment CKV2: Concentration in ppm of molybdate, vanadate and calcium in the solution plotted against the residence time. In this experiment the pH was initially not reduced, but at t = # min. the pH was reduced to about # by the addition of nitric acid. 49

4-12 Experiment CSN - image of the formed particles as viewed under the microscope. Left an image taken after # min. and right after # min. 50

4-13 Experiment CK - image of the formed particles as viewed under the microscope. Left an image taken after # min. and right after # min. 50

5-1 Block diagram of the salt sludge separation process. 54

5-2 Ternar phase diagram of the $NaNO_3$,Na_2SO_4 and water system. The eutectic line of $Na_2SO_4 \cdot 10H_2O$ and ice is indicated by the blue line, the feed composition is indicated by the red circle and the crystallization path is represented by the red line. 56

5-3 Gravity settler for the separation of liquid- solid mixtures [47] 72

6-1 Sodium nitrate concentrated product stream purity and mass flow for a varying crystallizer operating temperature. 79

6-2 Sodium sulfate decahydrate product purity and mass flow for a varying crystallizer operating temperature. 79

6-3 Ice product purity and mass flow for a varying crystallizer operating temperature. 80

6-4 Sodium nitrate concentrated product stream purity and mass flow for a varying feed flow. 81

6-5 Net profit for a varying crystallizer operating temperature. 83

6-6 Flow diagram of the process design for the salt sludge separation, including heat integration. 86

7-1 Flow diagram of the process as described in the second case study: A cooling crystallizer is configured in series with an EFC crystallizer. 90

7-2 Flow diagram of the process as described in the third case study: Two EFC crystallizers connected in series. 91

7-3 Prospect of generated profits of the processes of case studies 1 to 3 for 35 operating years. The purple lines shows the loss for the case when the brine is untreated and discharged. 95

List of Tables

1-1 Simplified brine compositions depending on the base that is used. 3

3-1 Overview of the EFC batch experiments. 25
3-2 Solubility data ternary system of sodium nitrate, sodium sulfate and water found in literature. 27
3-3 Solution compositions used for the experiments with the sodium ternary system together with the expected eutectic temperature and compounds that are expected to crystallize. 29
3-4 Experimental results of solutions S1 to S4, SM, SMV1 and SMV2. The steady state temperature is shown in the second column. The concentration of the respective compounds in the solution is shown in the other columns together with the error (including the error of the IC or ICP). A '-' indicates that a component was not present in the solution. 31
3-5 Solubility data of the ternary system of potassium nitrate, potassium sulfate and water found in literature. 34
3-6 Solution compositions used for the experiments with the potassium ternary system together with the expected eutectic temperature and compounds that are expected to crystallize. 36
3-7 Experimental results of solutions K1 to K5, KM, KMV and KS. The steady state temperature is shown in the second column. The concentration of the respective compounds in the solution is shown in the other columns together with the error (including the error of the IC or ICP). 37

4-1 Starting composition of the solutions used in the precipitation experiments together with the pH of solution after the calcium oxide was dosed, the residence time and the dosage of calcium oxide. 46
4-2 Mean particle size for experiment CSN 50

5-1 Quotations for two cooling machines with similar operating temperatures but different capacities. 70

5-2 Quotations for two buffer vessel width different volumes. 71
5-3 Quotations of two vacuum belt filters of different sizes. 73

6-1 Costs and Revenue for the process with optimized operating temperature for a feed flow of #m^3/hr. 84
6-2 Numerical results for the heat integration between the bleed stream and the process stream. 85
6-3 Numerical results for the process design with and without heat integration for a feed flow of #m^3/hr.. 87

7-1 Annual product flow, purity and value per tonne of product for the three cases. The recovery for each component is given as amount of pure product vs. the amount of feed of that component 93
7-2 Numerical results for case study 3, shown next to the results of the previous case study and original process 94

Chapter 1

Introduction

For confidentiality purposes, most results have been left out of this report

Spent hydrotreating catalysts are considered one of the most hazardous wastes generated in oil refineries [9][8]. Coming from the hydrotreating process, in which sulfur, nitrogen and other unwanted compounds are removed from a fuel[1][3], the spent hydrotreating catalysts consists mainly of alumina (the structure of the catalyst), molybdenum and nickel or cobalt (the active layers on the alumina structure) and the deposited compounds that caused the catalyst to become inactive. These are vanadium, (heavy) hydrocarbons, carbon (coke) and sulfur (as metal sulfides and as part of the coke)[6][7]. Beside the toxic metals, the iron sulfides in the spent catalyst are pyrophoric and may ignite spontaneously in the presence of air, coke and sunlight [9], causing a real concern for refineries regarding the storage of the spent catalyst, especially when considering that a large scale refining company generates nearly 500 tons of spent catalyst per year [9].

Due to strict environmental regulations and high costs that involve the safe deposition of spent hydrotreating catalysts, the refining industry is looking for new methods to process the spent catalysts into less hazardous waste and valuable products[6]. As the levels of molybdenum and, depending on the spent catalyst, also vanadium can be high (Mo, 10-15% and V, 5-10%), spent hydrotreating catalyst could be a potential source for these valuable metals [8]. Therefore HyVent Technology has developed a new process for the reclamation of molybdenum and vanadium from spent hydrotreating catalysts.

The conventional metal recovery process consists of a roasting step where the carbon and sulfur are removed from the spent catalyst as CO2 (g) and SO2 (g) by oxidation with air, followed by a metal reclaim step using pyro-lurgic methods, e.g. smelting, and by chemical leaching methods with different types of chemicals. This process and related current global processes have substantial environmental, regulatory and economic disadvantages. The process developed by HyVent differs from conventional methods in that it combines the carbon and sulfur oxidation with the leaching of metals in one step. This has advantages relating to cost, environment and regulations. However, this process produces a mixed alkali metal sulfate and nitrate brine which must be treated.

Handling an alkali metal sulfate and nitrate brine, either for the recovery of the inorganic material, or for the reduction of the waste stream, is very energy intensive and costly [10]. It is, however, of great importance that the brine is treated properly as brine disposal has a negative impact on the environment due to the potential groundwater contamination.
Although there are several methods available for the treatment of brine, crystallization-based separation processes can be applied as the solute concentrations in the mixture are high. A huge disadvantage of evaporative crystallization, however, is the high energy requirement to evaporate the water and cooling crystallization is limited by the remaining solubility of the inorganic material at low temperature. Membrane crystallization techniques have many advantages, but are limited by scaling on the membrane surface and are therefore limited to a certain solute concentration. Above all, these methods produce a final salt product that is always contaminated with other salts. This makes the successful separation of the salt waste product very unlikely [11]. Consequently, novel treatment technologies are required. A novel technology that has shown promising results in the treatment of brine is Eutectic Freeze Crystallization (EFC).

1-1 Research objective: A new concept for separation of salt sludge produced by the HyVent metal recovery process

A crucial feature in the HyVent process is the treatment of the discharged brine from the HyVent metal recovery process. Therefore this thesis focuses on the development of a process that has the ability to recycle the water to the process, minimize residual brine discharge and to recover the salts as concentrated brine or solid products (sulfate and nitrate salts). The aim is to achieve a ZLD process (zero liquid discharge), where no water should leave the process in the form of a waste stream.
In figure 1-1 a block diagram is shown representing the HyVent metal recovery process with spent hydrotreating catalysts as feed and a mixed alkali metal sulfate and nitrate brine as output, followed by the salt sludge separation process, of which the design is the main goal of this thesis.

The brine is a mixture of potassium or sodium nitrate and sulphate and will contain some residual molybdenum and vanadium. The brine discharged by the metal recovery process is acidic with a pH of around #, so in order to reduce the cation-anion imbalance and reduce the acidity of the stream, the feed is neutralized with either sodium hydroxide (NaOH) or potassium hydroxide (KOH). Eutectic freeze crystallization will be applied to separate the alkali metal nitrate and sulphate products and attempts will be made

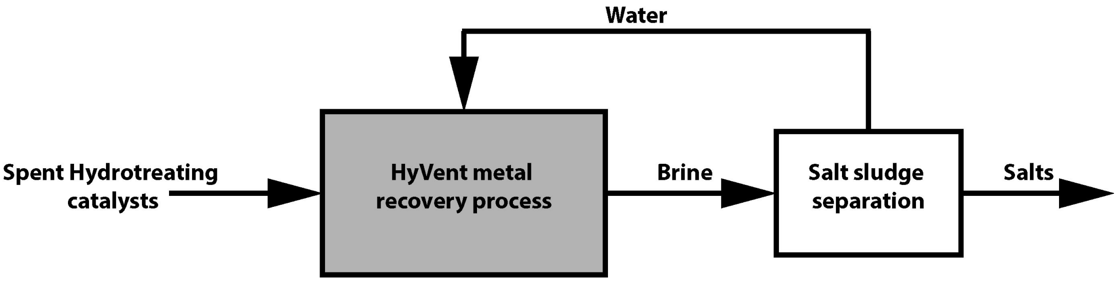

Figure 1-1: Block diagram representing and the salt sludge separation process

to precipitate the molybdate and vanadate out of the brine by the addition of calcium hydroxide. The ability to separate the brine into water and separated alkali metal nitrate and sulphate solid products (or concentrates) with very low residual molybdenum and vanadium content, has a substantial impact on the operating cost of the process and this will determine the base of choice (NaOH or KOH). The salts products can be sold to e.g. the fertilizer industry and the process water can be fed back to the metal recovery process as wash water.

Depending on the base that is used, the composition of the brine is different. For this thesis the brine is simplified to an aqueous solution with a composition as provided in table 1-1.

Table 1-1: Simplified brine compositions depending on the base that is used.

Base NaOH	Base KOH
$NaNO_3$	KNO3
Na_2SO_4	K_2SO_4
MoO_4	MoO_4
VO_3	VO_3

The salt sludge separation process is depicted as a black box in figure 1-2 and a process needs to be developed for it in order to achieve the desired products with the specified input stream. The following constraints for the process design are formulated:

- As eutectic freeze crystallization is a promising technology for the separation of brine into recyclable and usable fractions, the salt recovery process should include an **Eutectic Freeze Crystallization** process.
- The input process stream has a pH of # to #, and therefore neutralization with either **Sodium Hydroxide** or **Potassium hydroxide** is required. The final choice between the two bases is dependent on the results of the economical evaluation of the process design.

- The salt recovery process is a **Zero Liquid Discharge (ZLD)** process, i.e. all water is either recycled back to the HyVent process or is part of one of the products (e.g. in a concentrated solution of one of the components). No water can be discharged as waste.
- The sulfate and nitrate salts (as sodium or potassium salts) are the main products and are required to meet certain purity standards.

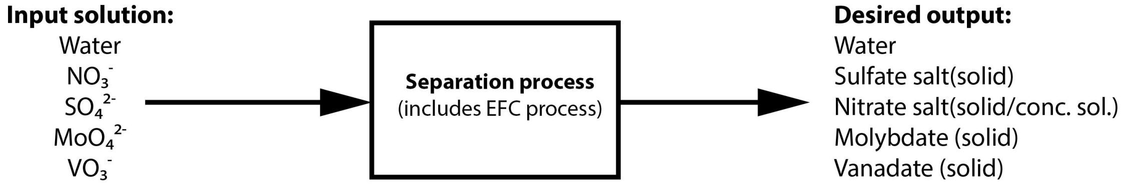

Figure 1-2: Black box process with specified input stream and desired output.

With the general objective to design the salt recovery process and the given constraints of this process, a main research question can be formulated:

Is EFC a viable method to separate aqueous solutions of sodium nitrate and sodium sulfate, or potassium nitrate and potassium sulfate, in the presence of molybdate and vanadate traces, into pure compounds, while ensuring a zero liquid discharge process?

In order to answer this research question a number of sub questions are formulated:

- What are the eutectic points of the different (sodium and potassium) nitrate, sulfate and water systems and what is the influence of traces of molybdenum and vanadium on these points in terms of temperature and composition?
- What ice purity can be obtained from the EFC process and is post treatment of the water/ice required?
- What sodium or potassium sulfate salt purity can be obtained from the EFC process?
- What sodium or potassium nitrate product purity can be obtained and is further treatment required?
- To what extend can calcium hydroxide be used to precipitate the molybdate and vanadate traces out of the solution?
- What process design options for a continuous process can be identified?

- What is the best choice of base given the re-usability of the salts and what is the best process design in terms of energy consumption, cost of equipment and raw material costs?

To answer these sub questions, a series of EFC experiments was conducted as well experiments where calcium hydroxide was added to precipitate the molybdate and vanadate traces out of the solution. With the experimental results a process model was developed in which different process designs were economically evaluated and a final process design could be chosen.

1-2 Structure of the thesis

In figure 1-3 the structure of this thesis is visualized in a diagram. First, in chapter 2 the fundamentals of eutectic freeze crystallization and crystallization in general are covered. In order to study the separability of the brine with EFC, the EFC experiments are covered in chapter 3. The remaining process stream needs to be cleared of the molybdenum and vanadium traces, which is achieved by calcium precipitation experiments and are discussed in chapter 4. With the obtained experimental results, the development of the process model for the salt sludge separation is discussed in chapter 5 and in chapter 6 a number of case studies is formulated and elaborated upon in order find the final process design for the salt sludge separation process.

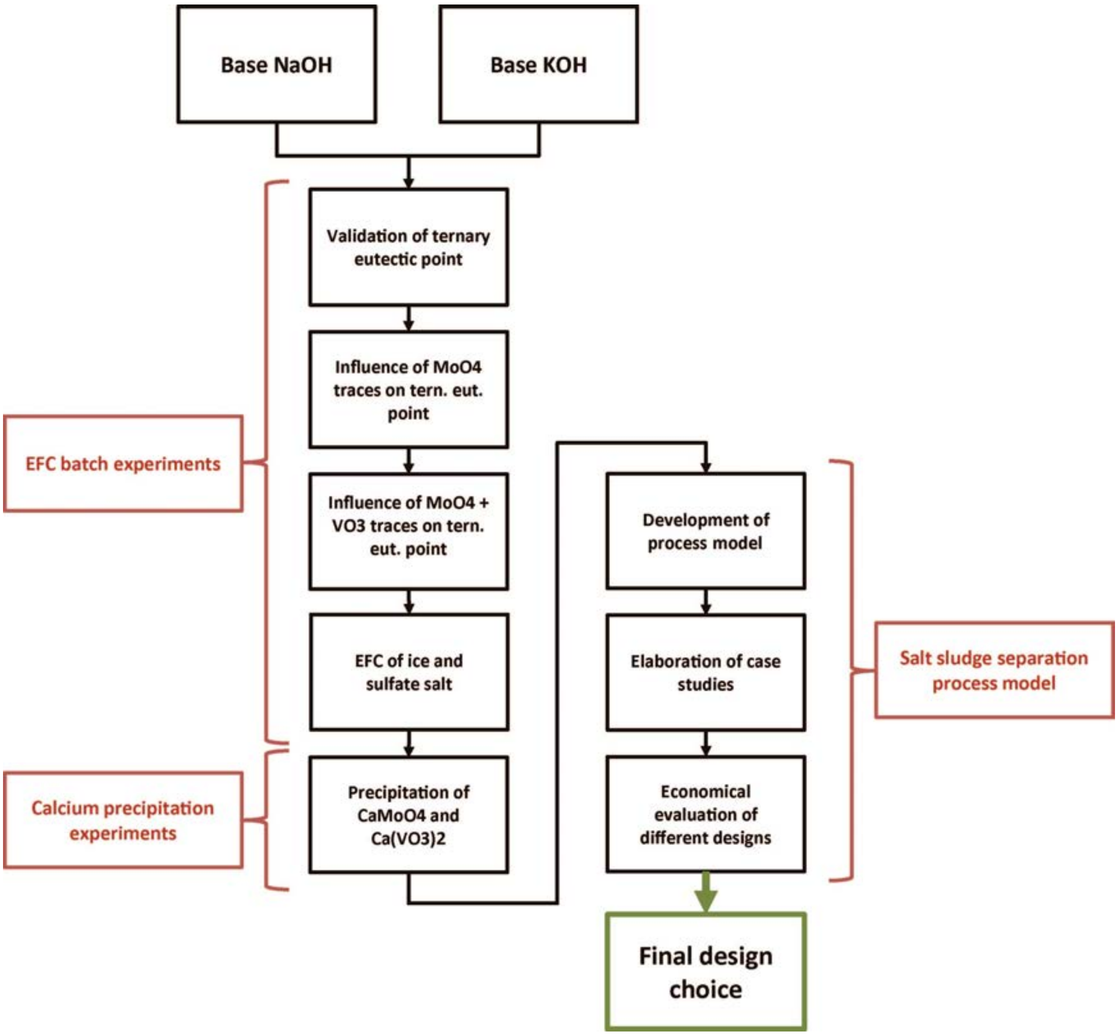
Base NaOH
Base KOH
Validation of ternary eutectic point
Influence of MoO4 traces on tern. eut. point
Influence of MoO4 + VO3 traces on tern. eut. point
EFC of ice and sulfate salt
Precipitation of CaMoO4 and Ca(VO3)2
EFC batch experiments
Calcium precipitation experiments
Development of process model
Elaboration of case studies
Economical evaluation of different designs
Salt sludge separation process model
Final design choice

Figure 1-3: Schematic overview of the thesis

Chapter 2

Eutectic freeze Crystallization

For confidentiality purposes, most results have been left out of this report

Eutectic freeze crystallization, as the term suggests, is a crystallization technology operating at the eutectic point of a solution. It is used to separate solvent and solute compounds simultaneously from a solution. Though, before a more detailed explanation can be given, first the basic principle of crystallization and its phenomena should be addressed.

2-1 Crystallization

Crystallization is a physical process that can be defined as a phase change in which a solid product is formed from a solution [12] and can be applied as a separation technology. A solution is a mixture of one or more solid solute compounds that are dissolved in a liquid solvent. In aqueous solutions this solvent is water. A solution always thrives to be in phase equilibrium and therefore thrives to be either unsaturated or saturated for the solute compound. In a solution that is supersaturated the solute concentration is higher than the solubility of the solute in the solvent at the given temperature and pressure. This is a thermodynamically unfavourable situation, as the solution has shifted away from the phase equilibrium. In order to restore equilibrium the concentration of the solute has to be reduced and, at a constant temperature, this can only be achieved by the crystallization of the solute.
In figure 2-1 a typical solubility curve of a binary solution is shown. Solubility represents the equilibrium concentration of the system as a function of temperature and for many solutes the solubility increases proportionally to the temperature. The solution with a composition and temperature that is located below the solubility curve is an unsaturated

solution and likewise, a solution above the solubility curve would be supersaturated. A solution with a concentration (c) and temperature as in point A is thus supersaturated and, as was mentioned before, this solution is thermodynamically unstable. In order to return to a stable condition, the composition of the solution needs to decrease by crystallization of the solute until a saturated solution is obtained and equilibrium is restored (point B, concentration = c^*). The crystallization of the solute in this super saturated solution happens spontaneously, i.e. no work or heat has to be added to the system, and as this process is isothermal, a vertical path is followed from point A to point B.

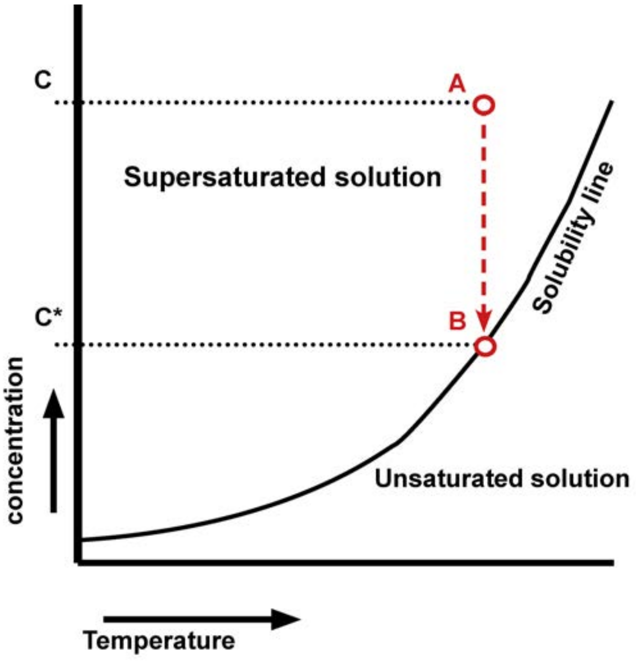

Figure 2-1: Basic phase diagram of a binary system.

2-1-1 Supersaturation

Supersaturation is the driving force for a crystallization and can be defined as deviation of a solution from thermodynamic equilibrium[13] with a crystalline phase. A solution is in thermodynamic equilibrium with a crystalline phase if the chemical potentials of the solute (μ_L^*) and crystalline phase (μ_S^*) are equal[13]:

$$\mu_L^* = \mu_S^* \tag{2-1}$$

Supersaturation can then be expressed as:

$$\Delta\mu = \mu_L - \mu_S^* = \mu_L - \mu_L^* \tag{2-2}$$

Where μ_L is the chemical potential of the solution that is no longer in equilibrium with the crystalline phase.
As chemical potential changes proportionally to the concentration [15], supersaturation can be expressed as the difference in concentration of the (supersaturated) solution (c) and the concentration of a saturated solution at the same temperature and pressure as the supersaturated solution (c*):

$$\Delta c = c - c^* \tag{2-3}$$

Another common way to express the supersaturation is as a ratio: the supersaturation ratio S:

$$S = \frac{c}{c^*} \tag{2-4}$$

In order to better understand the relation between crystallization and supersaturation, a closer look has to be taken at the kinetic processes behind crystallization.

2-1-2 Nucleation

Crystallization can best be described as a two step process: in a supersaturated solution first a minute solid body, a nucleus, is created, after which this nucleus accommodates crystal growth and the nucleus grows into a crystal. Two different nucleation mechanisms can be identified:

1. Primary nucleation, the formation of nuclei in a system that initially contains no crystals of the same compound.
2. Secondary nucleation, nucleation induced by crystals that are already present in a supersaturated system.

Primary nucleation

Primary nucleation (and nucleation in general) is a complex process and can only occur under sufficient supersaturation. Primary nucleation itself can also be categorized into two different types of nucleation: Homogeneous nucleation, which is spontaneous nucleation, and heterogeneous nucleation, which is nucleation on the surface of impurities or other non-solute particles in the system. It can best be understood by looking at the free energy that is involved in this process.

The relation for the energy that is involved in the formation of a solid phase and the creation of a surface of a spherical cluster of molecules is given by [13]:

$$\Delta G = 4\pi\gamma r^2 + 4\frac{\pi}{3}\Delta G_v r^3 \tag{2-5}$$

$$\Delta G = \Delta G_{Surf} + \Delta G_{Vol} \tag{2-6}$$

Where r is the cluster diameter, ΔG is the excess Gibbs free energy related to the formation of the solid body, ΔG_v is the change in Gibbs free energy related to the phase change to a solid. γ is the interfacial energy between the crystal surface and the surrounding supersaturated solution. The right hand side of equation 2-5 can be split into two parts: the first part represents the energy that is related to surface of the cluster of molecules (ΔG_{Surf}) and the change in energy is proportional to r^2. The second part represents the energy related to volume of the cluster (ΔG_{Vol}) and, as $\Delta G_v = -v_m^{-1} ln(S)$, is negatively proportional to r^3. In figure 2-2 equation 2-5 is shown for an increasing cluster radius. The energy related to the surface and volume of the cluster are plotted separately in figure as well.

From equation 2-5 it becomes clear that the behaviour a formed spherical cluster of solute molecules depends on the size (r) of the cluster, i.e. it can either redissolve or grow into a larger particle. Both cases (growth or redissolving) result in the decrease in the total free energy of the cluster. In figure 2-2 can be observed that for a small cluster size the overall free energy is governed by the surface energy of the cluster and has a positive value. However, as the cluster size increases, the energy related to the volume of the cluster becomes more dominant and the overall free energy reaches a maximum value, after which it decreases rapidly. At the maximum value of the overall free energy, the energy contributions of both surface and volume of the cluster are in equilibrium and the cluster radius corresponding to this point is the critical radius: clusters with a radius below the critical radius are unstable and tend to dissolve in the solution, while clusters with a radius above the critical radius are considered stable and will grow into crystals.

As the energy contributions of both surface and volume of the cluster are in equilibrium for a cluster with a critical radius, the derivative of ΔG is zero at this cluster radius. Therefore, the derivative of equation 2-5 to the cluster radius can be rewritten as an expression for the critical nucleus size [13] [14]:

$$\frac{d\Delta G}{dr} = 8\pi\gamma r + 4\pi\Delta G_v r^2 = 0 \tag{2-7}$$

$$r_c = \frac{-2\gamma}{\Delta G_v} = \frac{2M\gamma}{\rho RT ln(S)} \tag{2-8}$$

Where ρ is the crystal density, S is the ratio of supersaturation and M is the molar weight of the solute.

The free energy that corresponds to the critical cluster nucleus size can be obtained by substituting equation 2-8 in equation 2-5:

$$\Delta G_c = \frac{16\pi\gamma^3}{3\Delta G_v^2} = \frac{4\pi\gamma r_c^2}{3} \tag{2-9}$$

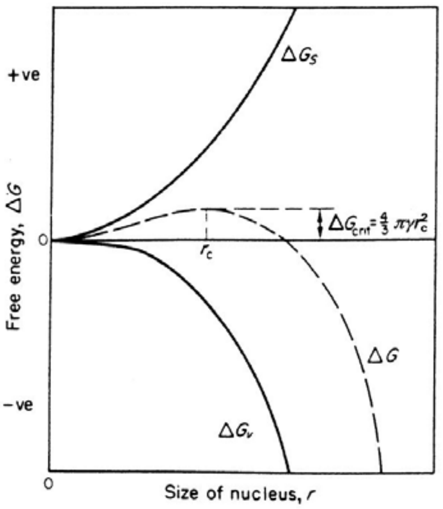

Figure 2-2: Gibbs free energy diagram for homogeneous nucleation showing the critical nucleus radius. [14]

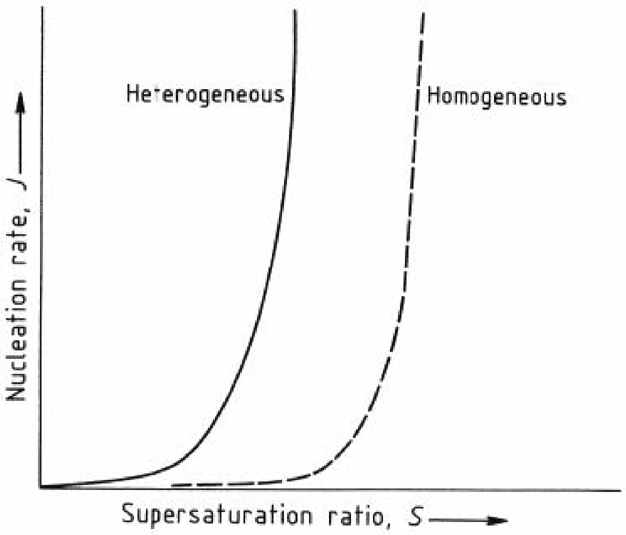

Figure 2-3: Effect of supersaturation on the homogeneous and heterogeneous nucleation rates. [13]

The nucleation work required to create a nucleus can be obtained by substituting equation 2-8 into equation 2-5[13]:

$$W^* = \frac{16\pi\nu^2\gamma^3}{3k^2T^2ln^2(S)} \tag{2-10}$$

With ν the molar volume, k the Boltzmann constant and S the supersaturation ratio. The nucleation work is the energy barrier that needs to be overcome in order for nucleation to occur. The nucleation rate J can be related to the nucleation work by expressing it in the form of an Arrhenius reaction rate equation with A as a pre-exponential factor and J the nucleation rate as the amount of nuclei per unit of volume per unit of time:

$$J = A\ exp\Big(-\frac{W^*}{kT}\Big) = A\ exp\Big(-\frac{16\pi\nu^2\gamma^3}{3k^3T^3ln^2S}\Big) \tag{2-11}$$

Equation 2-11 is the nucleation rate for homogeneous nucleation. The expression for the nucleation rate for heterogeneous nucleation (eq. 2-12 [13]) is similar to this equation.

The difference lies in the pre-exponential factor for heterogeneous nucleation, A$_{HEN}$, and the effective interfacial energy, γ_{ef}. The effective interfacial energy is smaller than the interfacial energy for homogeneous nucleation, as for heterogeneous nucleation the cluster of molecules that forms the nucleus is positioned on the surface of a non-solute particle (impurity particle or surface of the crystallization vessel). This effectively reduces the surface of the cluster that is in contact with the supersaturated solution and in this way the free energy term that is related to the volume of the cluster (Δ G$_{Vol}$) becomes dominant at a smaller cluster size. Therefore, as shown in figure 2-3, at the same supersaturation ratio the nucleation rate for heterogeneous nucleation is higher than for homogeneous nucleation.

$$J = A_{HEN}\ exp\Big(-\frac{W^*_{HEN}}{kT}\Big) = A\ exp\Big(-\frac{16\pi\nu^2\gamma^3_{ef}}{3k^3T^3ln^2S}\Big) \tag{2-12}$$

True spontaneous (homogeneous) nucleation is considered to be an uncommon event, as it is nearly impossible to obtain a solution that is completely free of foreign particles. Therefore, after careful examination, spontaneous nucleation is often induced by the presence of foreign particles and is actually heterogeneous nucleation.

Metastable zone

Although primary nucleation can occur at any amount of supersaturation, a stable nucleus is much more likely to form at a higher level of supersaturation. The equation for the nucleation rate (eq. 2-11) confirms this statement as it depends exponentially on the supersaturation ratio: once a critical level of supersaturation is exceeded, the nucleation rate increases extremely fast. As supersaturation is defined as the concentration difference above the saturation concentration, this critical level supersaturation can be visualized in a solubility diagram (fig. 2-4): A line can be drawn parallel to the solubility curve in the supersaturated region. This curve is called the metastable zone limit, the area between the two curves is called the metastable zone and although the solution is supersaturated in this zone, primary nucleation is still unlikely to occur. Once the composition of a solution at a certain temperature reaches the metastable zone limit the supersaturation has reached the critical level and primary nucleation will occur at a very fast rate.

Secondary nucleation

Secondary nucleation takes place if crystals of the solute are already present. Different types of secondary nucleation can be specified: Small crystals can be added to a supersaturated solution (Seeding), inducing crystal growth of these seed crystals.

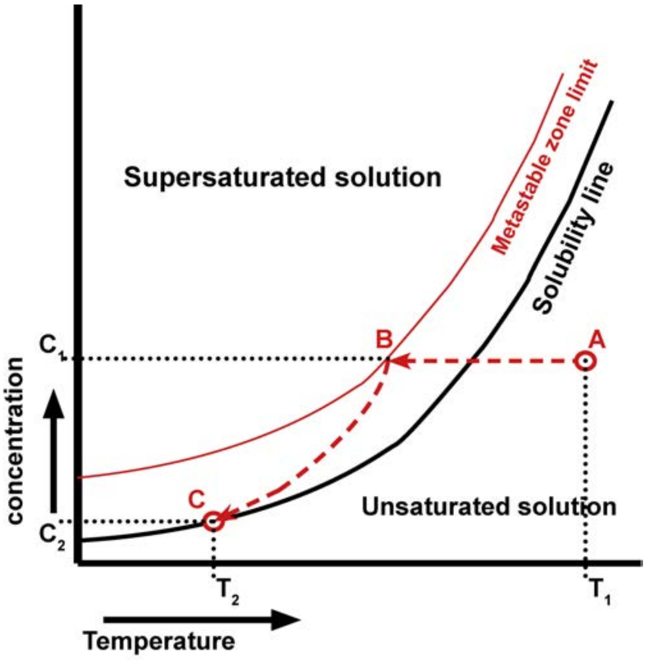

Figure 2-4: Basic phase diagram of a binary system in which the metastable zone limited is shown as the red line parallel to the black solubility curve. Furthermore, the crystallization path of a typical cooling crystallization process is shown.

Contact nucleation is another type of secondary nucleation and can be described as the formation of new crystals by the collision of crystals with the wall, with the stirrer blades in the crystallizer (attrition) or with other crystals of the same compound. This type of secondary nucleation only occurs when the crystals that are already present are of a sufficiently large size [13].

2-1-3 Crystal growth

Once a stable nucleus has formed, the next stage of the crystallization process can occur, which is the growth of a nucleus into a crystal of visible size. As for nucleation, supersaturation is the driving force for crystal growth. Crystal growth determines the final crystal size and shape, it also has a significant effect on the purity of the crystalline product [12].

Crystal growth can be described as a two-step process in which first a cluster of solute molecules is transported to the surface of the crystal by means of mass transfer in the form of diffusion or convection. This step is followed by the integration of the cluster of solute molecules into the crystal lattice.

2-1-4 Crystallization methods

For crystallization from solution different methods can be identified and are described below:

Cooling crystallization

Cooling crystallization can be applied to systems in which the solubility of the solute compound is a (steep) function of temperature, i.e. the solubility changes proportionally to the temperature. A typical phase diagram of such a system is shown in figure 2-4. A solution with a composition (C_1) and temperature (T_1) in the unsaturated region is chosen (point A) and this solution is cooled down to a final predetermined temperature (T_2). During the cooling process the path form point A to point B is followed: the clear solution crosses the solubility curve and becomes supersaturated and when the metastable zone limit is reached, primary nucleation occurs. This starts the crystallization process and as the solute compound crystallizes out of the solution, the concentration of the solution decreases (path from point B to point C) until the solution has reached the final temperature and has consumed all its supersaturation in point C.
The starting temperature and final temperature should be chosen at the steepest part in the solubility curve, as in that case a relatively large amount of crystalline product can be formed.
The main disadvantage of cooling crystallization is that the solubility of the solute compound at the lowest temperature limits the yield and a part of the solute is always lost in the remaining mother liquor. This loss can , however, be reduced by applying post treatment steps to recover more of the solute compound.[13]

Evaporative crystallization

In evaporative crystallization the amount of solvent in the solution is reduced by means of evaporation. In this way the solute concentration increases and eventually the solution becomes saturated. When the metastable zone is reached, primary nucleation takes place and subsequently crystal growth commences. From this point on, the solvent evaporation rate is balanced by the crystal growth rate. The yield is therefore directly related to the solvent evaporation. This type of crystallization is ideal for solute compounds which solubility is hardly temperature dependent or for very soluble compounds, where cooling crystallization becomes uneconomically.[13]
The main disadvantage of evaporative crystallization is the high energy demand for the evaporative process.

Precipitation

In a precipitation process two soluble compounds are mixed together to form an insoluble compound and therefore, precipitation is applied for the production of hardly soluble compounds.
As the reactant streams are relatively concentrated, the supersaturation achieved are relatively high upon mixing the streams. Especially at the inlet of the reactant streams to the precipitation vessel supersaturations become very high and this consequently results in rough crystal growth and the formation of unwanted/unexpected solid phases, such as amorphous materials.[13]

Other crystallization methods

Other common crystallization methods that will not be further discussed in this document are: Anti-solvent crystallization and vacuum crystallization.[13]

2-2 Separation principle of eutectic freeze crystallization

Eutectic freeze crystallization (EFC) is a technology to separate inorganic aqueous solutions into pure ice and pure solidified solutes simultaneously by operating at the so called eutectic point [16]-[20]. EFC is based on a combination of different types of crystallization and can best be described with use of a phase diagram. In figure 2-5 a typical phase diagram of a binary system consisting of water and a dissolved salt is depicted.

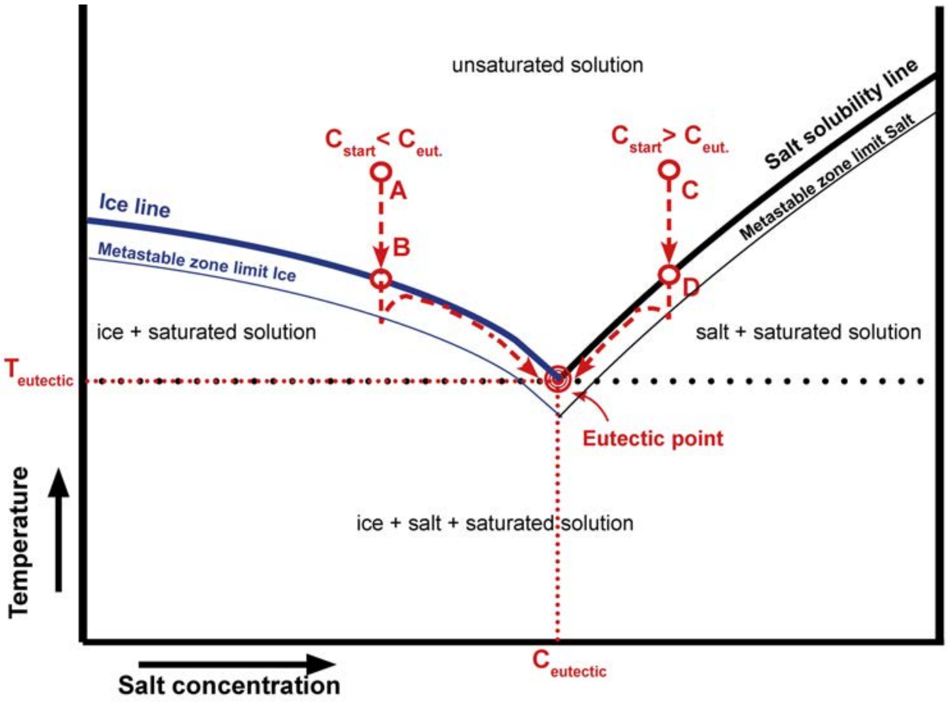
unsaturated solution
Salt solubility line
Metastable zone limit Salt
$C_{start} < C_{eut.}$
$C_{start} > C_{eut.}$
A
B
C
D
Ice line
Metastable zone limit Ice
ice + saturated solution
salt + saturated solution
$T_{eutectic}$
Eutectic point
Temperature
ice + salt + saturated solution
Salt concentration
$C_{eutectic}$

Figure 2-5: Typical phase diagram of an inorganic aqueous solution.

The solution is cooled and proportionally to the temperature the solubility decreases. Depending on the starting concentration of the solution, different paths through the phase diagram are followed:

Cooling a solution with a starting composition as in point **A** will reach the freezing point (point **B**) of the solution before the salt solubility line is reached. Upon further cooling the solution becomes subcooled and eventually ice crystals start to form (freeze crystallization). The crystallization of the solvent causes the solute concentration to increase and, upon further cooling, the composition of the solution follows the path on the ice line from point **B** to the point where the ice line and the salt solubility line intersect, the so called **eutectic point**. The solution becomes supersaturated in salt as well and once the metastable zone limit of the salt is crossed, the salt also starts to crystallize. With both the solvent and solute compounds crystallizing, the solution finds

an equilibrium at the eutectic point with a corresponding eutectic temperature. Further cooling of the eutectic solution results in the simultaneous crystallization of the solvent and solute, while the solution stays at constant composition and temperature.
Cooling a solution with a starting concentration as in point **C** will first reach the salt solubility line (point **D**). Further cooling causes the solution to become supersaturated in salt and once the metastable zone limit of salt is crossed the salt starts to crystallize (cooling crystallization). The crystallization of the solute causes the concentration of the solute to decrease and upon further cooling the composition of the solution follows the path on the salt solubility line from point **D** to the eutectic point. There the solvent becomes supersaturated as well and ice starts to crystallize. Again, the solution finds an equilibrium at the eutectic point.
This example shows that regardless of the starting composition, cooling a eutectic system of a binary solution of a salt and water, eventually leads to an equilibrium in composition (and temperature) in the eutectic point.
The two solid phases (ice and crystallized salt) are separated from each other by simply using gravitational forces: Salt crystals generally have a larger density than the solution and sink to the bottom, while the density of ice is lower and rises to the surface (fig. 2-6). The top product is a slurry of ice and mother liquor, which contains no or only traces of the crystalline salt. The bottom product is a slurry of salt crystals and mother liquor. The separation of the solid phases from the mother liquor can be done with typical solid-liquid separators (e.g. filters, centrifuges etc.).

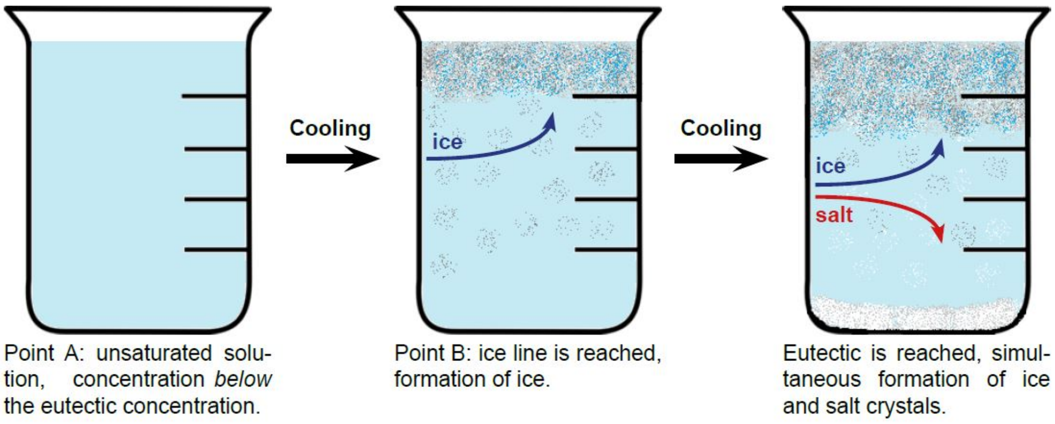
Cooling
ice
Cooling
ice
salt
Point A: unsaturated solution, concentration *below* the eutectic concentration.
Point B: ice line is reached, formation of ice.
Eutectic is reached, simultaneous formation of ice and salt crystals.

Figure 2-6: Schematic representation of the EFC process

2-3 EFC process for ternary systems

In the previous section the EFC process is described for a binary system, which can give a clear and understandable explanation of the process. In reality however, most industrial streams contain multiple salts and the system becomes more complex. Therefore, with the support of an example, EFC for a ternary system will be explained.

In figure 2-7 a ternary system of compounds H_2O, Q and R is depicted, where water is the solvent and both Q and R are solute compounds. The diagram is a projection on which the temperature of the equilibrium points are given, so the temperature axis can be imagined as the axis perpendicular to the surface of this thesis. Two eutectic solubility lines can be identified, where two solid phases are in equilibrium with the solution: The line from the binary eutectic point of R and water at point BP' towards the ternary eutectic point, point D. On this line water and R are in equilibrium. The other eutectic line comes from the binary eutectic point of Q and water at point BQ' towards the ternary eutectic point. Two more lines can be drawn: One from the ternary eutectic point towards the 100% R point (left corner) and another from the ternary eutectic point towards the 100% Q point (right corner). This divides the diagram in four areas: In the top area ice is the crystallizing compound, in the right area Q, in the left area R and in the bottom area both R and Q are crystallizing. The ternary eutectic point is the intersection of these four lines and therefore, at this point, all three components are in equilibrium with each other. In the case that a solution with composition A is cooled down, the first compound that will crystallize is water as A is located in the area where ice is the crystallizing compound. Continuously cooling the solution decreases the amount of water in the system, changing the composition according to the line from point A towards point B. Eventually the eutectic line of water and R is crossed and after trespassing the metastable zone limit of R, it starts the crystallize as well(point B). Upon further cooling the supersaturation of R is consumed, which causes the composition to go towards the eutectic line of water and R. The composition follows the path from point B towards point C . When the metastable limit of Q is trespassed (point C) this component also starts to crystallize. With all three components crystallizing, the solution will approach the ternary eutectic point (point D), where the solution reaches equilibrium. Further cooling at this point results in the simultaneous crystallization of all three compounds.

Note that, at the ternary eutectic point both the solute compounds crystallize and a mixture of these salts with low filterability and low added value settles. Therefore it is of higher interest to operate the process under conditions where only one solute compound (and ice) crystallize. In this example this means that the metastable zone limit of Q should not be reached. However, as two components crystallize out the concentration of the third component increases. Therefore, a bleed stream should be used in order to extract also Q and in this way reducing the amount of Q in the solution. The use of a bleed stream will be discussed in more detail later in this thesis.

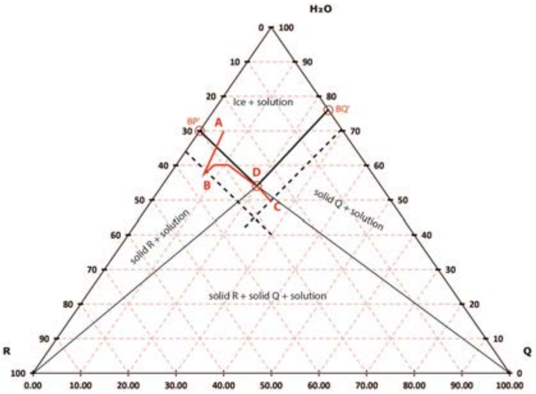

Figure 2-7: Ternary phase diagram of a sodium bicarbonate - sodium carbonate - water system

2-4 State of the art of EFC

The first studies on the eutectic freeze crystallization process for the disposal of brine were done by Stepakoff et al. (1974) [16], Barduhn et al. (1979) [17] and Swenne et al.(1979) [18]. These studies were done with direct cooling, where an inert cooling fluid is added to the solution and the evaporation of this fluid causes cooling of the solution. A drawback of this method is that the cooling fluid is present in all equipment and this leads to the production of fine ice and salt crystals, which require complex and expensive solid-liquid separation systems.
Therefore van der Ham and Witkamp (1998) started the development of an EFC process with indirect cooling, where the cooling liquid is not mixed with the solution, but flows through jackets and pipes. With the experimental setup with indirect cooling, the feasibility of EFC for the waste water treatment of aqueous solutions like $CuSO_4$, $NaNO_3$ and $NH_4H_2PO_4$ was proved [20] [19]. Since the high density difference between the ice and salt crystals, it was possible to conduct EFC and the separation of ice and salt crystals in one apparatus.
In 2003 experiments were done in a new type of crystallizer, which was developed by van der Ham and Witkamp: the cooled disk column crystallizer (CDCC, figure 2-8). This new type of EFC equipment was capable of crystallizing and separating ice and salt from an aqueous feed stream [21].

Following the work of van der Ham, Vaessen developed another type of EFC crystallizer: the scraped cooled wall crystallizer (SCWC) [22] [27]. In this type of crystallizer the walls were cooled instead of the disks inside the crystallizer as was the case in the CDCC (fig. 2-11). This resulted in a better gravitational separation of the ice and salt crystals, but other results were approximately equal to that of the CDCC.
A general model for continuous EFC in different scraped surface crystallizers based on

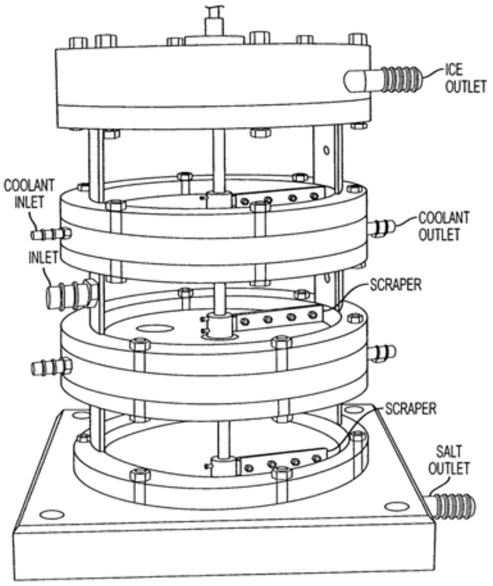

Figure 2-8: Schematic representation of a cooled disk column crystallizer.

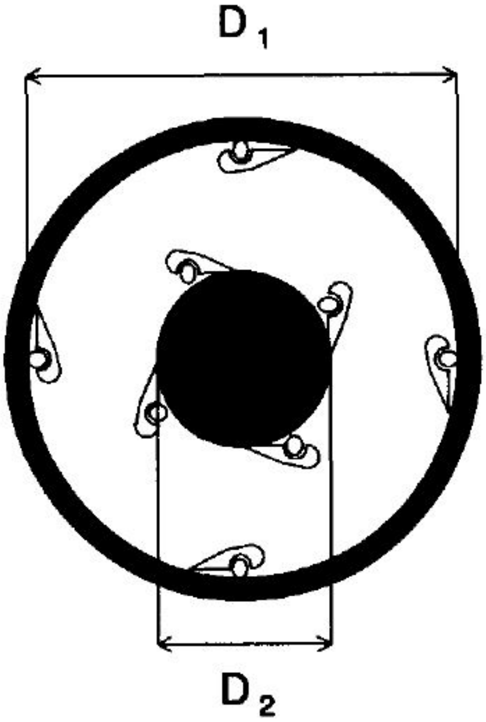

Figure 2-9: Cross sectional top view of the scraped cooled wall crystallizer.

population balances was developed by Himawan et al.(2004) [28] [29]. With this model an evaluation of current EFC crystallizer designs could be performed and provide a framework for the model based design, analysis and optimization of eutectic type of crystallizers.
Genceli et al.(2005) developed scaled up versions of the cooled disk column crystallizer (CDCC-2 and CDCC-3, fig. 2-10) with a capacity of 220 liter and did research to understand nucleation and growth on cooled surfaces, theoretically and experimentally in relation to the prevention of scale formation. Also a model for fast implementation of EFC technology in the industry was suggested [30] [31] [32].
Rodriguez Pascual et al [24] presented a novel Scraped Cooled Wall Crystallizer (SCWC-2) with a scraped heat exchanger optimized for higher heat transfer and for efficient gravitaional separation to increase the throughput. This crystallizer has volume 200 liter and contains multiple heat exchanger modules (fig. 2-12). This setup was used for EFC experiments with the ternary system $NaHCO_3$-Na_2CO_3-H_2O [25].

In 2010 Lewis et al. [34] designed a EFC process for a multi component waste water stream. Modeling tools were applied to describe complex saline systems under different process conditions and experiments were conducted to validate the model. Randall et al.

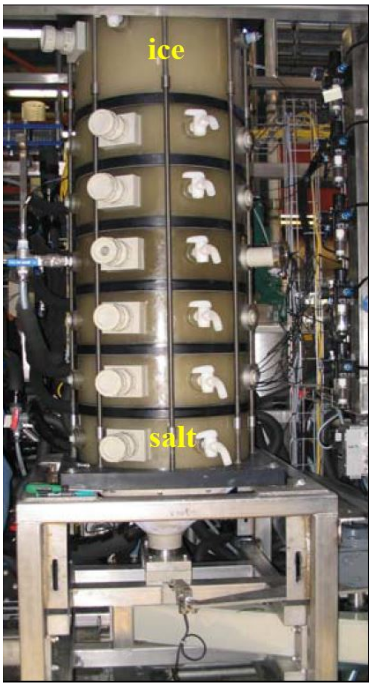

Figure 2-10: Scaled up version of the cooled disk column crystallizer.

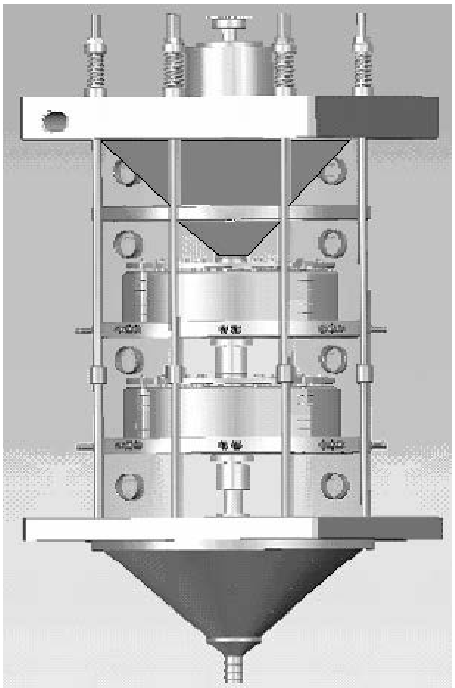

Figure 2-11: Cross sectional top view of the scraped cooled wall crystallizer.

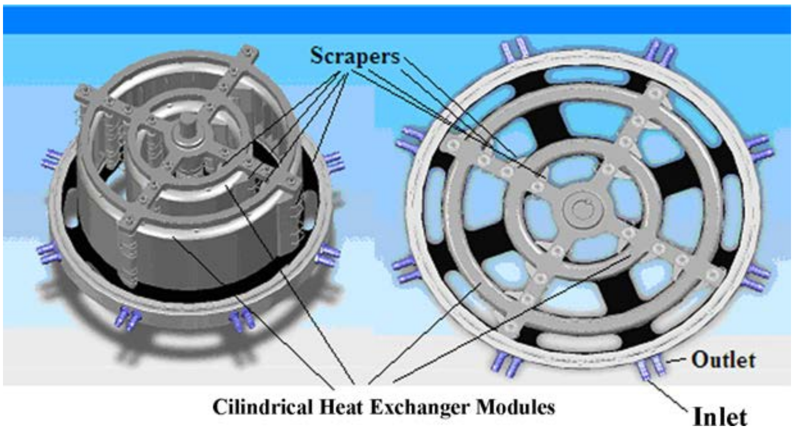

Figure 2-12: Heat exchanger module of the scaled up scraped cooled wall crystallizer.

[35] did a case study on the treatment of a reverse osmosis brine with EFC. Brine samples of a RO plant were used in these experiments. A conversion 97% of the brine sample was recovered as pure water and pure salts(calcium sulphate 98.0% purity and sodium sulphate 96.4% purity). The overall recovery of water was calculated to be 99.9%.

Chapter 3

EFC batch experiments

For confidentiality purposes, most results have been left out of this report

As eutectic freeze crystallization is a requirement for the process design, the black box diagram of figure 1-2 can be replaced by the block diagram depicted in figure 3-1. In this block diagram, a base, either sodium hydroxide or potassium hydroxide, is added to the stream and subsequently, the process stream is treated by EFC separation. Ideally the EFC crystallizer produces pure water in the form of ice, one of the compounds (sodium or potassium nitrate or sulfate) as a pure solid and the remaining compound as a concentrated solution of that compound. It is essential that both compounds do not crystallize simultaneously as in that case a mixed salt product is obtained, which is genuinely worthless.
However, as it is unknown to what extend the separation of the process can be achieved by only EFC, a series of experiments have to be conducted. Only after the insight from these experiments any further pre- or post-treatment steps can be developed. The EFC experiments are discussed in this chapter.

In order to study the separability of the process stream by using eutectic freeze crystallization, the crystallization behaviour of the different compounds in the solution has to be studied. A series of batch experiments is conducted in a 1L EFC setup. As a guidance, a number of sub questions are formulated, which can be answered by the experimental results.

1. What are the eutectic points of the different systems and what is the influence of traces of Molybdenum and Vanadium on these points?

PFD-simple_EFC.jpg

Figure 3-1: Option 1: EFC process only.

  - First, the eutectic points of the pure ternary systems of sodium nitrate, sodium sulfate and water, and potassium nitrate, potassium sulfate and water are experimentally identified and compared to the data found in literature.
  - Secondly, the influence of the addition of # ppm of Molybdate on the eutectic points of the ternary systems is experimentally analysed.
    - How does the temperature of the eutectic point change?
    - How does the composition of the eutectic point change?
    - Will the Molybdenum stay in the solution, will it form a solid solution with the sulfate salt or will it crystallize on its own with the sodium or potassium?
  - Thirdly, the influence of the addition of # ppm of Molybdate and # ppm of Vanadate on the eutectic of the ternary systems is experimentally analysed.
    - How does the temperature of the eutectic point change?
    - How does the composition of the eutectic point change?
    - Will the Molybdenum and Vanadium stay in the solution, will they form a solid solution with the sulfate salt or will they crystallize on their own with the sodium or potassium?

2. What ice purity can be obtained and is post treatment of the ice/water required?
   - What purity can be obtained without washing of the ice?
   - What purity can be obtained with washing of the ice with subcooled water?
   - To what degree is mother liquor included in the ice crystals?

3. What salt purity can be obtained and what are the options for re-use?
    - What purity can be obtained without washing of the salts?
    - What purity can be obtained with washing of the salt?
    - What is the uptake of Molybdenum and/or Vanadium in sulfate and nitrate salts?

Six sets of batch experiments are conducted and an overview of these experiments is given in table 3-1

Table 3-1: Overview of the EFC batch experiments.

Experiment set	Base	System
1	NaOH	Pure ternary system of sodium sulfate, sodium nitrate and water
2	NaOH	Addition of traces of Molybdate to pure sodium system
3	NaOH	Addition of traces Molybdate + traces of Vanadate to pure sodium system
4	KOH	Pure ternary system of potassium sulfate, potassium nitrate and water
5	KOH	Addition of traces of Molybdate to pure potassium system
6	KOH	Addition of traces Molybdate + traces of Vanadate to pure potassium system

3-1 Experimental setup for the EFC batch experiments

The batch experiments are conducted in a 1 liter glass beaker placed inside a cooling jacket provided by EFC Separations B.V. The use of an overhead anchor stirrer ensures homogenous mixing of the solution in the crystallizer. Temperature measurement is done by PT-100 probes connected to a controlled ASl F250 precision thermometer with an accuracy of ± $0.01°C$ and a resolution of ± 0.001 $°C$. The probes are measure the temperature of the coolant and the solution. Temperature logging is done via a computer using the program LabView. Cooling is provided by a Tamson cooling machine with a temperature range from -80 $°C$ to 20 $°C$ and the cooling medium that is used is methanol. The ice and salt crystals are washed and filtered on glass filters.

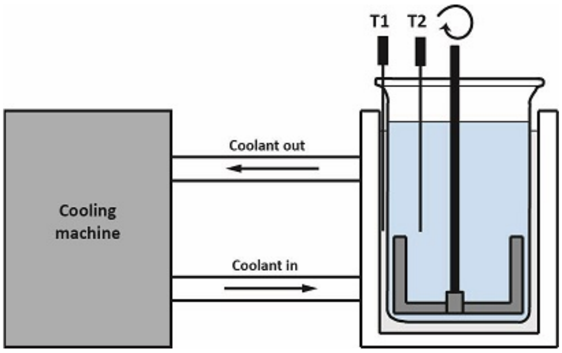

Figure 3-2: Schematic representation of the experimental setup used in the batch experiments.

3-2 Batch experiments with aqueous solutions of sodium sulfate and sodium nitrate

The first set of batch experiments are conducted with a solution of sodium sulfate and sodium nitrate dissolved in demineralized water. In these experiments molybdate and vanadate, which are present the HyVent process stream are not added to the solution. The purpose of this experiment is to study the crystallization behaviour of the ternary system of water, sodium nitrate and sodium sulfate, and compare the results with those found in literature. Another important goal of this experiment is to study the separability of the sulfate and nitrate salts, as good separability of these salts is an essential aspect of the to be designed recovery process.
In the second set of experiment traces of molybdate are added to the pure system of experiment set 1. The aim of these experiments is to study where and in what form the molybdate precipitates. Will it crystallize together with another salt and end up in its crystal lattice or, ideally, will it stay in solution?
In the third set of experiments traces of both molybdate and vanadate are added to the pure ternary system of experiment set 1. The aim of these experiments is to study the influence of both molybdate and vanadate traces on the ternary eutectic point of sodium nitrate, sulfate and water and experiments were done to study the uptake of molybdate and/or vanadate in the sulfate and nitrate salts.

3-2-1 Solubility data and phase diagram of the sodium system

For the successful process development of the recovery process, good understanding of the phase diagram of the sodium nitrate, sodium sulfate and water system is required. As a phase diagram of this ternary system was not available, one had to be constructed from solubility points found in literature.
In literature [38] the following solubility points were found (table 3-2):

Table 3-2: Solubility data ternary system of sodium nitrate, sodium sulfate and water found in literature.

	$NaNO_3$ [w%]	**Na_2SO_4** [w%]	**T** [$°C$]	Eutectic point or eutectic line
1	0	3.7	-1.2	binary eut. point H_2O - $Na_2SO_4.10H_2O$
2	8.99	2.82	-4	point on eut. line H_2O - $Na_2SO_4.10H_2O$
3	25	1.32	-10.6	point on eut. line H_2O - $Na_2SO_4.10H_2O$
4	37.70	0.12	-17.8	ternary eut. point H_2O - $Na_2SO_4.10H_2O$ - $NaNO_3$
5	38	0	-18.1	binary eut. point H_2O - $NaNO_3$

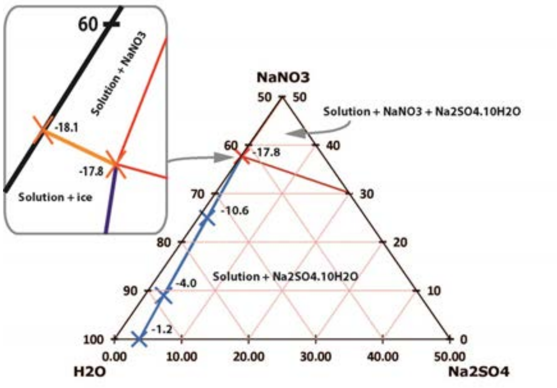

Figure 3-3: Ternary phase diagram of the Na_2SO_4, $NaNO_3$, H_2O system. The blue and orange lines resemble the eutectic lines of $Na_2SO_4 \cdot 10H_2O$ - H_2O and $NaNO_3$ - H_2O respectively.

With these solubility points a phase diagram as shown in figure 3-3 was constructed: In this ternary phase diagram a line is drawn through solubility points 1 to 4 from table 3-2, so starting at the binary system of sodium sulfate and water (point 1), increasing the nitrate content until the composition at the ternary eutectic (point 4) is reached. This line represents the eutectic line, where sodium sulfate decahydrate and water are in equilibrium. Another eutectic line can be drawn from point 5 to point 4 and on this line sodium nitrate is in equilibrium with water. The two eutectic lines cross in the so called ternary eutectic point, at which all three the components are in equilibrium.

For the addition of sodium molybdate to the ternary system of sodium nitrate, sodium sulfate and water, there is no solubility data available for the resulting quaternary system in literature. However, there is high probability that the molybdate traces will have an effect on the solubility of nitrate and sulfate salts.

The solubility information that was found included[38]:

- For the sodium molybdate only the eutectic data is available for the binary system with water: Eutectic temperature of -7.3°$C$with a composition of 24.7 w% Na_2MoO_4.
- for the ternary system of Na_2MoO_4, Na_2SO_4 and water literature states that a solid solution is formed between 0°C and 10°C.
- for the ternary system of Na_2MoO_4, $NaNO_3$ and water only solubility data is available at a temperature of 25°C at which $Na_2MoO_4 \cdot 2H_2O$ and $NaNO_3$ precipitate.
- For the quaternary system of Na_2MoO_4, $NaNO_3$, Na_2SO_4 and water no solubility data is available.

There is no solubility information available for the ternary system of sodium nitrate, sodium sulfate and water with molybdate for sub-zero temperatures, the region where EFC is applied, and it is therefore very difficult to predict the crystallization behaviour of the solutions used in this set of experiments. However, as literature states that a continuous solid solution is formed in the temperature range of 0 - 25 °C for the aqueous solution of sodium sulfate and sodium molybdate, it is possible that this behaviour continues in the sub-zero temperature region. This could result in the loss of molybdate in the crystal lattice of sodium sulfate decahydrate. The experiments will have to show if molybdate will end up in the sulfate crystal lattice and if so, to what extend the sulfate salts are contaminated with molybdate.

For the system of sodium nitrate, sulfate and water with vanadate even less solubility data is available. According to the concept of freezing point depression [40], addition of vanadate traces should result in the depression of the ternary eutectic point in terms of temperature and increase in composition of nitrate and sulfate. Other than this it is difficult to predict the effect of vanadate and molybdate traces.

3-2-2 Experimental procedure and solution compositions

In order to validate the solubility data found in literature, four solutions were prepared with compositions that are on the eutectic line of sodium sulfate decahydrate and water (solutions S1 to S4), see table 3-3. Furthermore, experiments were done where molybdate was added to the solutions with the ternary eutectic composition (solution SM) and after that also experiments where molybdate and vanadate were added (solutions SMV1 and SMV2). The uptake of molybdate and vanadate in the sodium sulfate decahydrate crystal lattice was studied in another experiment (solution SS).

Table 3-3: Solution compositions used for the experiments with the sodium ternary system together with the expected eutectic temperature and compounds that are expected to crystallize.

Solution	$NaNO_3$ [w%]	Na_2SO_4 [w%]	Na_2MoO_4 [w%]	$NaVO_3$ [w%]	Exp.T_{eut} [$°C$]	Expected solid compounds
S1	0	3.7	-	-	-1.2	$Na_2SO_4.10H_2O$ and ice
S2	20	2.28	-	-	-8.8	$Na_2SO_4.10H_2O$ and ice
S3	30	0.85	-	-	-13.21	$Na_2SO_4.10H_2O$ and ice
S4	37.7	0.12	-	-	-17.8	$Na_2SO_4.10H_2O$, ice and $NaNO_3$
SM	37.7	0.12		-	-17.8	$Na_2SO_4.10H_2O$, ice and $NaNO_3$
SMV1	37.7	0.12			-17.8	$Na_2SO_4.10H_2O$, ice and $NaNO_3$
SMV2	37.7	0.12			-17.8	$Na_2SO_4.10H_2O$, ice and $NaNO_3$
SS	8.90	2.80			-	$Na_2SO_4.10H_2O$ and ice

The same experimental procedure was followed for all the solutions. The solutions were prepared according to their compositions in a 1L glass beaker. The beaker was placed in the jacketed cooling vessel and the overhead stirrer was used until all salt particles were dissolved and an homogeneous solution was obtained. Solution SMV2, however, was filtrated as at neutral pH the # ppm of sodium vanadate did not dissolve completely and a filtrate was obtained with about # ppm of dissolved sodium vanadate.

The cooling machine was set to a temperature of $5°C$ below the expected eutectic temperature of the solution and the solution was cooled until crystallization of both ice and sodium sulfate decahydrate (for solutions S1 to S3) was observed or until the crystallization of all three components was observed (for solution S4,SM, SMV1 and SMV2). Once the desired components were crystallizing and the temperature of the solution had reached a steady value, a sample was taken of the mother liquor and the set temperature of the cooling machine was increased to about $0.5\ °C$ below this steady solution temperature [26], as cooling was only needed to compensate for heat losses to the environment. The solution was left to equilibrate for 20 hours, after which the stirrer was switched off in order for gravitational separation to take place between the ice and salt crystals. Once the salt crystals had settled, a sample of the mother liquor was taken and sampling of the solid products was commenced.

Ice samples were taken first and was done by filtrating about 5 grams of ice on a small glass filter. The first sample was left unwashed, the following five ice samples were washed with 1x5 ml; 2x5ml; 3x5ml; etc. subcooled water. The ice samples were melted and a sample of each melt was taken and diluted for analysis.

Salt samples were taken similarly but by washing with saturated solutions of the crystallized salt(s) at $20\ °C$. The salt samples were weighted and and dissolved in a known amount (mass) of demin water. The dissolved salt samples were diluted with deminwater and prepared for analysis.

All the samples were analysed using ion chromatography (IC) with an error of ±2.5% and/or inductively coupled plasma mass spectrometry (ICP).

3-2-3 Results and discussion

In figure 3-4 to 3-7 the temperature profiles are shown for the solutions S1 to S4. In the shown temperature profiles the first jump, the smaller jump, in temperature corresponds to the nucleation and crystallization of sodium sulfate decahydrate. After the formation of sodium sulfate has started, the solvent concentrates further until also ice starts to crystallize, indicated by the steep temperature increase.

For the solutions S1, S2 and S3 (fig. 3-4 to 3-6), the desired eutectic freeze crystallization was achieved, i.e. formation of both ice and sodium sulfate decahydrate, and the solution was left to equilibrate for 20 hours. This shown by the flat horizontal line. In figure 3-6, however, there was a mechanical issue with the stirrer and after 20 hours it was decided to warm up the solution slightly, after which cooling was recommenced and equilibrium was obtained after 40 hours.

In figure 3-7, solution S4, again only two crystallization peaks can be observed, eventhough all three components were crystallizing. It is possible that one of the salts only could reach low levels of supersaturation before it started to nucleate and therefore the temperature jump is too small to be observed.

Figure 3-4: Temperature profile of solution S1 with the time in hours on the x-axis and the temperature on the y-axis. The blue line represents the solution temperature, while the red line represents the coolant temperature.

Figure 3-5: Temperature profile of solution S2 with the time in hours on the x-axis and the temperature on the y-axis. The blue line represents the solution temperature, while the red line represents the coolant temperature.

Figure 3-6: Temperature profile of solution S3 with the time in hours on the x-axis and the temperature on the y-axis. The blue line represents the solution temperature, while the red line represents the coolant temperature.

Figure 3-7: Temperature profile of solution S4 with the time in hours on the x-axis and the temperature on the y-axis. The blue line represents the solution temperature, while the red line represents the coolant temperature.

The solutions samples at the end of each experiment had a composition as shown in table 3-4.

Figure 3-8: Ternary phase diagram of the Na_2SO_4, $NaNO_3$, H_2O system, in which the experimentally obtained eutectic points (orange) are shown together with those from literature (blue).

The experimental concentration of sodium sulfate of solution S1 and S4 corresponds well to those from literature (table 3-3, S1 and S4) as well as the temperatures of the found

Table 3-4: Experimental results of solutions S1 to S4, SM, SMV1 and SMV2. The steady state temperature is shown in the second column. The concentration of the respective compounds in the solution is shown in the other columns together with the error (including the error of the IC or ICP). A '-' indicates that a component was not present in the solution.

Solution	T [°C]	NaNO3 [w%]	Na_2-SO4 [w%]	MoO_4 [ppm]	VO_3 [ppm]
S1					
S2					
S3					
S4					
SM					
SMV1					
SMV2					

eutectic points. For S4 the concentration of sodium nitrate is about #% above that from literature, while the concentration of sodium sulfate is almost #% above that of literature. This can partly be explained by the literary data, which dates from 1930, when deep cooling and control of sub zero temperatures was relatively difficult compared to methods available today. Another reason is the calibration of the IC, which was not as accurate as was desired.

In figure 3-8 the results are plotted in the ternary phase diagram and it can be observed that the same trend is followed as that from literature with a slightly higher ternary eutectic point in terms of sodium nitrate sodium sulfate concentrations.

For the solution with traces of sodium molybdate, SM, the temperature of the ternary eutectic point has decreased slightly when compared to the pure system. This is as expected, as according to Thomsen et al. [40] addition of an extra compound often leads to freezing point depression. However, what is unexpected is the decrease of the sodium nitrate concentration of the eutectic point. This is more than # w% lower than that of the pure system. An explanation for this has proven difficult to find, as literature offers hardly any information on this system. An explanation could be the common ion effect as studies from Lewis et. al [33][34] have shown that the presence of 0.06m NaCl in a brine of sodium sulfate, decreased the solubility of the sulfate decahydrate ion. A similar effect might occur here with sodium nitrate and sodium molybdate, especially since the potassium system does not show this behaviour (as the results in the next section will show). In the potassium system sodium molybdate was added instead of potassium molybdate, therefore the common ion effect does not take place in this system. This is of course not a direct validation of the theory that the common ion effect causes the sodium nitrate concentration of the ternary eutectic point to decrease and a more detailed study should be conducted to find an explanation for this.

The sodium sulfate composition is hardly affected by the molybdate traces and only slightly increases due to the freeze point depression resulting from the addition sodium molybdate traces.

For the solutions with the sodium molybdate and sodium vanadate traces (SMV1 and SMV2) the temperature of the ternary eutectic point further decreased, as expected from freezing point depression. The sodium nitrate concentration is still lower than that of the pure system, but it increased slightly when compared to solution SM. As the same amount of molybdate trace are present as in experiment SM, in can be concluded that the vanadate traces cause the sodium nitrate concentration of the ternary eutectic point to increase again. The sodium sulfate concentration is also slightly lower than the pure system, but this could also be explained by the inaccuracy of the IC calibration, as the difference is only small.

The addition of # ppm of sodium molybdate and sodium vanadate clearly shows a further decrease in the sodium nitrate concentration, while the sodium sulfate concentration increased. This shows that there is a relation between the sodium nitrate and sulfate concentration and the molybdate/vanadate content, decreasing the sodium nitrate concentration for increasing concentrations of sodium molybdate

Ice and salt purity

In figure 3-9 the mean ice purity of solutions S1 to S4 is plotted against the amount of washing of the ice. As was expected, the purity increases with increasing amount of washing. After washing 3 times the purity is not much affected by more washing and the final purity of about # % was reached.

In figure 3-10 the mean ice purity of solutions SM and SMV1 is shown together with the molybdate and vanadate concentration of the ice product. In order to reduce the traces concentration below # ppm, at least one time washing is required. Further washing reduces the traces concentration to below #ppm and increases the ice purity to #%.

Assuming that all the sodium nitrate present in the ice comes from entrapped mother liquor, the fraction of mother liquor in the ice product can be estimated. This results in a mother liquor fraction of about #% in the ice product.

Figure 3-9: Mean ice purity (in %) of solutions S1 to S4 plotted against the amount of washing of the crystals with subcooled water, ranging from unwashed to 5x washing.

Figure 3-10: On the left y-axis the mean ice purity (in %) of solutions SM and SMV1 and on the right y-axis the concentration (in ppm) of molybdate and vanadate, both plotted against the amount of washing of the crystals with subcooled water.

In figure 3-11 the sodium sulfate decahydrate salt purity of solutions S1 to S3 is plotted against the amount of washing with saturated solution of the salt compound at 20°C. Washing increased the purity to about #%, while the unwashed salt only had a purity of # % of sodium sulfate decahydrate.

In figure 3-12 the sodium sulfate decahydrate salt purity of solution SS, so with molybdate and vanadate traces, is plotted against the amount of washing with water. Washing with water did not improve the purity of the sodium sulfate decahydrate product as this remained almost constant at #%. The sodium vanadate concentration remained constant as well, the sodium molybdate concentration decreased, after which it remained constant. Both the molybdate and the vanadate concentration in the salt are relatively high when compared to the mother liquor concentration of these two compounds. An explanation for this could be that washing with water, besides rinsing the sodium sulfate decahydrate crystal surface from mother liquor, caused a part of the sodium sulfate decahydrate salt to dissolve. In this way the amount of all the compounds in the salt product was reduced proportionally, leaving a product with about the same composition as the unwashed product. Therefore, washing with a solution that contains all the compounds but with a concentrations that are lower than that of the mother liquor, would most probably give better results in terms of sodium sulfate decahydrate purity and molybdate and vanadate concentrations in this salt. However, as the molybdate and vanadate concentrations are high when compared to that of the mother liquor, it can be assumed that a part of the sodium molybdate and also sodium vanadate, has formed a solid solution with the sodium sulfate decahydrate, as literature suggested [38]. Therefore, more research is required on how the molybdate and vanadate concentration in the sodium sulfate decahydrate product can be reduced.

Figure 3-13 and figure 3-14 show the purity of the formed salts from solutions SM and SMV1, respectively. For solution SM the salt consists for # % of sodium nitrate, washing steps increased this to #%. For solution SMV1 the unwashed salt consisted for #% of sodium nitrate and about #% of sodium sulfate decahydrate. Washing of the salt product increased the sodium nitrate concentration but not to a purity as high as for the salt from solution SM.

Figure 3-11: Mean sodium sulfate decahydrate salt composition from solutions S1 to S3. The salt composition (in w%) is plotted against the amount of washing of the crystals with a saturated solution of sodium sulfate, ranging from unwashed to 5x washing.

Figure 3-12: Sodium sulfate decahydrate salt composition from solution SS. The salt composition (in w%) is plotted against the amount of washing of the crystals with water, ranging from unwashed to 2x washing.

Figure 3-13: Salt composition from solution SM, The salt composition (in w%) is plotted against the amount of washing of the crystals with water.

Figure 3-14: Salt composition from solution SMV, The salt composition (in w%) is plotted against the amount of washing of the crystals with water.

3-3 Batch experiments with aqueous solutions of potassium sulfate and potassium nitrate

With the system of potassium nitrate, potassium sulfate and water experiments comparable to those with the sodium system were conducted: The fourth set of batch experiments (table 3-1) are conducted with a solution of potassium sulfate and potassium nitrate dissolved in demineralized water.

In the fifth experiment traces of molybdate are added to the pure system of experiment set 4 and in the sixth set of experiments traces of both molybdate and vanadate are added to the pure system of experiment set 4.

3-3-1 Solubility data and phase diagram of the potassium system

As for the ternary system with sodium, a phase diagram of the ternary system of potassium nitrate, potassium sulfate and water can be constructed from solubility points found in literature.

In literature [38] the following solubility points were found (table 3-5):

Table 3-5: Solubility data of the ternary system of potassium nitrate, potassium sulfate and water found in literature.

	$\mathbf{KNO_3}$	$\mathbf{K_2SO_4}$	**T** $[°C]$	Eutectic point or line
1	0	6.63	-1.8	binary eut. point H_2O - K_2SO_4
2	8.96	4.09	-3.32	ternary eut. H_2O - K_2SO_4 - KNO_3
3	9.42	0	-2.9	binary eut. H_2O - KNO_3

These solubility points can be used to construct a phase diagram as shown in figure 3-15: In this ternary phase diagram a line is drawn through solubility points 1 to 2 from table 3-5, so starting at the binary system of potassium sulfate and water (point 1), increasing the nitrate content until the composition at the ternary eutectic (point 2) is reached. This line represents the eutectic line, where potassium sulfate and water are in equilibrium.

Another eutectic line can be drawn from point 3 to point 2 and on this line potassium nitrate is in equilibrium with water.

The two eutectic lines cross in the ternary eutectic point, at which all three the compo-

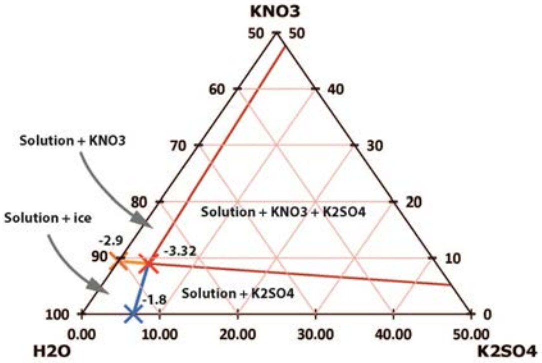

Figure 3-15: Ternary phase diagram of the K_2SO_4, KNO_3, H_2O system. The blue and orange lines resemble the eutectic lines of K_2SO_4 - H_2O and KNO_3 - H_2O respectively.

nents are in equilibrium.

Similar as for the sodium system, only little solubility data is available for the potassium system with molybdate traces. The following literature data was found [38]:

- For the potassium molybdate only the eutectic data is available for the binary system with water: Eutectic temperature of -38°C with a composition of 62.7 w% K_2MoO_4.
- For the ternary system of K_2MoO_4, K_2SO_4 and water only solubility data is available at a temperature of 25°C, at which continuous solid solutions are formed.
- For the ternary system of K_2MoO_4, KNO_3 and water only solubility data is available at a temperature of 25°C, at which both K_2MoO_4 and KNO_3 precipitate.
- For the quaternary system of K_2MoO_4, KNO_3, K_2SO_4 and water no solubility data is available.

Again, there is no solubility information available for the ternary (or quaternary) systems with molybdate for sub-zero temperatures. As was for the sodium system, literature states that a continuous solid solution is formed in the temperature range of 0 - 25 °C for the aqueous solutions of potassium sulfate and potassium molybdate. For the system of potassium nitrate, sulfate and water with vanadate even less solubility data is available.

3-3-2 Experimental procedure and solution compositions

The solubility data found in literature is again validated and four solutions were prepared with compositions that are on the eutectic line of potassium sulfate and water (solutions K1 to K4), see table 3-6. Experiments with traces of molybdate (solution KM) and both molybdate and vanadate (solution KMV) were conducted. The uptake of molybdate and vanadate in the potassium sulfate salt was studied in the experiment with solution KS. Note that, for the potassium system sodium molybdate and sodium vanadate were used instead of potassium molybdate and potassium vanadate, to reduce costs for the experiments. As such low quantities are used, the influence of the sodium ions on the potassium system can probably be neglected.

Table 3-6: Solution compositions used for the experiments with the potassium ternary system together with the expected eutectic temperature and compounds that are expected to crystallize.

Solution	KNO_3 [w%]	K_2SO_4 [w%]	Na_2MoO_4 [w%]	$NaVO_3$ [w%]	Exp.T_{eut} [$°C$]	Expected solid compounds
K1	0	7.1	-	-	-1.8	$K_2SO_4$and ice
K2	3	6.09	-	-	-2.31	K_2SO_4 and ice
K3	6	5.08	-	-	-2.82	K_2SO_4 and ice
K4	8.96	4.09	-	-	-3.32	K_2SO_4 and KNO_3 and ice
KM	7.297	3.551		-	-3.32	K_2SO_4 and KNO_3 and ice
KMV	7.88	3.62			-3.32	K_2SO_4 and KNO_3 and ice
KS	7.2	5.2			-	K_2SO_4 and ice

The same experimental procedure was followed as for the experiments with sodium.

3-3-3 Results and discussion

First of all, the potassium system was prone to excessive scaling of especially the potassium sulfate salt and the ice. This hampered the experiments, as it was not possible for all the solutions to let them equilibrate for the desired 20 hours. For some of the solutions the experiment had to be stopped after only 8 hours, simply due to the stirrer that got stuck in the scaling layer (see figure 3-16). Above this, the crystallization kinetics of the both the potassium sulfate and the potassium nitrate were relatively slow: In the sodium system equilibrium was in all cases reached in 2 hours. In the potassium system it took more than 6 hours to reach equilibrium and as was mentioned before, due to the scaling, experiments sometimes had to be stopped only minutes after equilibrium was reached.

Figure 3-16: Photo of the encountered scaling on the stirrer. The scale layer consists of mostly ice with potassium sulfate crystals. Similar scaling layers caused the beaker to break in other experiments with the potassium system.

A fifth solution (K5) was added to the list of solutions with the same starting composition of the fourth solution(K4) to validate these results. In figure 3-17 to 3-20 the temperature profiles are shown for the four solutions. Unfortunately, the temperature profile of the third solution was lost due to a failure of LabView.

In the temperature profiles of figures 3-17 and 3-18 the effect of the slow crystallization kinetics of potassium sulfate can be observed: The first temperature jump corresponds to the formation of ice, after which the temperature slowly decreases as the potassium sulfate concentrates. After some hours, the crystallization of potassium sulfate is marked by the slowly increasing temperature. Finally equilibrium is reached after several hours and the line becomes horizontal.

In figures 3-19 and 3-20, where solutions K4 and K5 were used, first crystallization of potassium nitrate is marked by a small temperature jump, after which ice also crystallizes. Again, potassium sulfate takes a while longer to crystallize.

Figure 3-17: Temperature profile of solution K1 with the time in hours on the x-axis and the temperature on the y-axis. The black line represents the solution temperature, while the red line represents the coolant temperature.

Figure 3-18: Temperature profile of solution K2 with the time in hours on the x-axis and the temperature on the y-axis. The black line represents the solution temperature, while the red line represents the coolant temperature.

Figure 3-19: Temperature profile of solution K4 with the time in hours on the x-axis and the temperature on the y-axis. The black line represents the solution temperature, while the red line represents the coolant temperature.

Figure 3-20: Temperature profile of solution K5 with the time in hours on the x-axis and the temperature on the y-axis. The black line represents the solution temperature, while the red line represents the coolant temperature.

The solutions samples at the end of each experiment had a composition as shown in table 3-7.

Table 3-7: Experimental results of solutions K1 to K5, KM, KMV and KS. The steady state temperature is shown in the second column. The concentration of the respective compounds in the solution is shown in the other columns together with the error (including the error of the IC or ICP).

Solution	T [$^\circ C$]	KNO_3 [w%]	K_2SO_4 [w%]	MoO_4 [ppm]	VO_3 [ppm]
K1					
K2					
K3					
K4					
K5					
KM					
KMV					

Figure 3-21: Ternary phase diagram of the K_2SO_4, KNO_3, H_2O system, in which the experimentally obtained eutectic points (orange) are shown together with those from literature (blue).

The experimental concentration of potassium sulfate of solution 1, 4 and 5 deviate slightly from those from literature. The temperatures of the found eutectic points correspond much better to the literary values. The concentration of potassium nitrate of the ternary eutectic point (solution 4 and 5) is about # w% lower than literature suggests. This can again be explained by inaccuracy of the IC calibration and the literary data, which dates from 1930, similar to as was explained for the sodium experiments.
In figure 3-21 the results are plotted in the ternary phase diagram and it can be observed that the same trend is followed as that from literature (blue/gray crosses) with a slight bending in the eutectic line of potassium sulfate and water.
For the solution with traces of molybdate, KM, a temperature decrease can be observed for the ternary eutectic point when compared to that of solution K5. The potassium nitrate concentration has increased slightly, which is expected according to freeze point depression. The potassium sulfate concentration slightly decreased.
The addition of both molybdate and vanadate caused the temperature of the ternary eutectic point to decrease further and increase the potassium nitrate and potassium sulfate concentration, as expected according to freezing point depression.

Ice and salt purity

In figure 3-22 the mean ice purity of solutions K1 to K5 is plotted against the amount of washing of the ice. The purity increases with increasing amount of washing and after washing 3 times the purity is not much affected by more washing and is above # % .
In figure 3-23 the mean ice purity of solutions Km and KMV is shown together with the molybdate and vanadate concentration of the ice product, both are plotted against the amount of washing. As was the case for the sodium system, at least one time washing is required in order to reduce the molybdate and vanadate concentration to below # ppm. Further washing increases the purity and reduces the molybdate and vanadate concentration of the ice.

Figure 3-22: Mean ice purity (in %) of solutions K1 to K5 plotted against the amount of washing of the crystals with subcooled water, ranging from unwashed to 5x washing.

Figure 3-23: On the left y-axis the mean ice purity (in %) of solutions KM and KMV and on the right y-axis the concentration (in ppm) of molybdate and vanadate, both plotted against the amount of washing of the crystals with subcooled water.

It proved difficult to take multiple salt samples form an experiment, as a large part of the formed salt ended up in the scale layer of ice. Therefore it was not always possible to do as many washing steps as was desired. In figure 3-24 the potassium sulfate salt purity of solutions K2 and K3 (For solution K1 not enough salt samples could be taken) is plotted against the amount of washing with saturated solution of the salt compound at $20°C$. Only one washing step was done and this increased the potassium sulfate salt purity from #% to #%.
In figure 3-25 the potassium sulfate salt purity of solution KS is plotted against the amount of washing with water. Washing improved the potassium sulfate salt purity from #% to #% and low concentrations of potassium molybdate and potassium vanadate, although these were not much affected by the washing.
Figure 3-26 and figure 3-27 show the purity of the formed salts from solutions KM and KMV, respectively. As expected, the salt composition represents the composition of the mother liquor and potassium nitrate and potassium sulfate have formed in the ratio 3:1 respectively. Washing with water did not have much effect on the composition of the formed salts.

Figure 3-24: Mean potassium sulfate salt composition from solutions K2 and K3. The salt composition (in w%) is plotted against the amount of washing of the crystals with a saturated solution of potassium sulfate, ranging from unwashed to 5x washing.

Figure 3-25: Potassium sulfate salt composition from solutions KS. The salt composition (in w%) is plotted against the amount of washing of the crystals with water, ranging from unwashed to 2x washing.

Figure 3-26: Salt composition from solution KM, The salt composition (in w%) is plotted against the amount of washing of the crystals with water.

Figure 3-27: Salt composition from solution KMV, The salt composition (in w%) is plotted against the amount of washing of the crystals with water.

3-4 Conclusions

The pure ternary systems of sodium nitrate, sodium sulfate and water, and potassium nitrate, potassium sulfate and water have been studied in a series of batch experiments and were successfully compared to literary data. The found eutectic points were similar to those found in literature and showed the same trends.
Addition of # ppm of molybdate to the pure systems have shown that the ternary eutectic point of potassium nitrate, potassium sulfate and water is only slightly affected by the molybdate traces and behaved as was expected in terms of freezing point depression. The molybdate traces did have a significant effect on ternary eutectic point of sodium nitrate, sodium sulfate and water, as the composition of sodium nitrate decreased by more than 6 w%. The temperature, however, decreased as was expected according to freezing point depression.
Addition of # ppm of both molybdate and vanadate traces further decreased the temperature of the ternary eutectic point of potassium nitrate, potassium sulfate and water and increased the potassium nitrate concentration of this point. For the sodium system it increased the sodium nitrate concentration of the ternary eutectic point of sodium nitrate, sodium sulfate and water when compared to the results of the addition of only molybdate traces, but the concentration was still below that of the pure sodium system. The effect on the sodium sulfate concentration of the ternary eutectic point was insignificant.
Increasing the molybdate and vanadate traces to # ppm further decreased the sodium nitrate concentration while increasing the sodium sulfate concentration of ternary eutectic point of sodium nitrate, sodium sulfate and water.

The ice samples and subsequent washing of these samples have shown that with washing of three times the sample volume a purity of above # % can be obtained for the sodium system, and above #% for the potassium system.
Sodium sulfate decahydrate and potassium sulfate crystals had a purity above #% for a solution with composition on the eutectic line of water and sodium/potassium sulfate. For the sodium sulfate decahydrate crystals the molybdate and vanadate concentrations were high compared to the concentration of the mother liquor and therefore it can be assumed that a part of the sodium molybdate has integrated in the crystal lattice of the sodium sulfate salt. In order to improve the quality of the sodium sulfate decahydrate salt the effect of other washing options should be studied.
For the potassium sulfate crystals the molybdate concentration is just below # ppm and vanadate concentration about # ppm.

Furthermore, the experiments with the potassium system were prone to scaling of ice and potassium sulfate. Also, the crystallization kinetics were much slower when compared to the sodium system: Where the sodium system reached a steady EFC process in 1 to 2 hours, it took more than 6 hours for the potassium system to reach steady state. No excessive scaling was encountered for the sodium system.

3-4-1 Implications for the process design

The ice product can be recycled to the HyVent metal recovery process and depending on the purity requirements of the recycle water, washing of the ice can be implemented to improve the purity from about #% to #%. A mother liquor of about #% was found in the ice product

The sulfate salt product has purity above #%, however, for the sodium sulfate product the quality might prove insufficient due to the molybdate and vanadate concentration which is still high. The quality of the salt product effects the process design economically as the selling price decreases for a lower product quality.

The block diagram of figure 3-1 can be extended with the findings from the batch experiments and a new block diagram is shown in figure 3-28.

With the validated phase diagrams of sodium system and the potassium system, an operating point of the EFC crystallizer can be chosen: For a sharp separation of the sulfate and nitrate compounds, an operating point on the eutectic line of water and sodium/potassium sulfate, close to but just above (in terms of temperature) the ternary eutectic point has to be chosen. In this way sodium/potassium sulfate is the only crystallizing solute. Furthermore, operating close to the ternary eutectic point results in a minimal sodium/potassium sulfate concentration in the remaining sodium/potassium nitrate solution.

For the sodium system the sodium sulfate concentration in the sodium nitrate concentrated solution is around #w%, which is sufficiently low for the sodium nitrate product. In the potassium nitrate concentrated solution, however, the potassium sulfate concentration is around #w%. This implicates the use of a post treatment step to decrease the sulfate content of the potassium nitrate product and on the other hand increasing the potassium sulfate yield. A case study will have to point out the relevance of a post treatment step for the recovery of potassium sulfate.

A post treatment step that is required for both systems is one that decreases the molybdate and vanadate content in the sodium/potassium nitrate concentrated solution. This treatment will be discussed in the next chapter.

Figure 3-28: Block diagram of the process with the implemented results from the EFC batch experiments.

Chapter 4

Removal of molybdate and vanadate as precipitates of calcium

For confidentiality purposes, most results have been left out of this report

In the previous chapter the recovery of the sodium or potassium sulfate product and water by the use of eutectic freeze crystallization was discussed. The sodium or potassium nitrate rich stream that leaves the EFC crystallizer, the bleed stream, still contains the molybdate and vanadate traces. Depending on the base that is used (NaOH or KOH), the stream also contains sodium or potassium sulfate. These are traces for the sodium system (about # w% Na_2SO_4) or a significant amount of sulfate for the potassium system (about # w% K_2SO_4). In order to recover the sodium or potassium nitrate, these contaminants have to be removed. Besides, for the potassium system a post treatment step has to be introduced to recover the remaining potassium sulfate from the potassium nitrate product, but this will discussed in the next chapters

A method to precipitate molybdate and vanadate out of the process stream is by the addition of calcium to the stream (fig. 4-1), as both calcium molybdate as calcium vanadate have a solubility that is far below that of calcium hydroxide and that of calcium sulfate. However, in literature not much has been reported on the precipitation of molybdate and vanadate from alkaline solutions of sodium or potassium sulfate and nitrate. There are, however, many patents that claim the successful separation of molybdate and vanadate from alkaline solutions [43][44][45]. Some of these patents come from the metallurgical industry, while others from alternative methods to treat spent hydrotreating catalysts. Below, the solubility of different calcium components in water are listed[38], note that the units of the solubility of calcium molybdate are in milligrams per 100 ml instead of grams per 100 ml. Solubility data of calcium vanadate could not be found, but different patents [44][45] stated that it is below that of calcium molybdate:

- $CaOH = 0.173$ g/100 ml
- $CaNO_3 = 56.39$ g/100 ml
- $CaSO_4 = 0.201$ g/100 ml
- $CaMoO_4 = 0.0022$ mg/100 ml
- $Ca(VO_3)_2$ = below that of calcium molybdate

`PFD-calcium_prec.jpg`

Figure 4-1: Block diagram representing the removal of molybdate and vanadate form the concentrated nitrate stream by the addition of calcium hydroxide.

Calcium can be added in the form of calcium oxide, however, as calcium oxide dissolves into calcium hydroxide and thus a strong base, adding it to the process stream will increase the pH of the stream. If desired, this pH increase can be neutralized by the addition of nitric acid.
In order to study if and to what extend precipitation with calcium can be used to remove the molybdate and vanadate from the nitrate rich solution, a series of experiments will be conducted. These experiments will answer the following sub questions:

- To what extend can molybdate and vanadate be taken out of the solution with this precipitation step?
- What dosage of calcium hydroxide is required and what is the effect of overdosis?
- To what extend will sulfate precipitate as calcium sulfate?

- What is the influence of pH on the precipitation of calcium molybdate and calcium vanadate (and calcium sulfate)?
- As calcium molybdate and calcium vanadate likely precipitate as very fine crystals, do the crystals settle and if so, what is the settling time of the formed crystals?

4-1 Experimental setup for the calcium precipitation batch experiments

The batch experiments are conducted in a 100 ml glass beaker placed on a stir plate, which ensures homogenous mixing of the solution in the beaker. The pH and temperature measurement is done by a Greisinger GMH 3500 pH meter. The used chemicals, i.e. calcium oxide, sodium and potassium sulfate, sodium and potassium nitrate, sodium molybdate and sodium meta vanadate are bought from Sigma Aldrich. The samples and calcium precipitates are filtered on glass filters.

`schem_calcium.jpg`

Figure 4-2: Schematic representation of the experimental setup used in the calcium precipitation experiments.

4-2 Experimental procedure

A series of small scale batch experiments was conducted both for the sodium system as for the potassium system. Each experiment started with a 50 ml solution with a composition of the corresponding ternary eutectic point and the solutions that were used are listed in table 4-1.

During each experiment the desired amount of calcium oxide was added to the solution and the mixture was continuously stirred. The starting pH of the solution was around #, the addition of calcium oxide caused the pH to go to around a pH of #. PH neutralization was done by addition of nitric acid to the mixture. Sample analysis was done by ICP analysis.

4-2-1 Effect of calcium dosage and pH

In order to study the effect of calcium oxide dosage and pH of the solution on the precipitation of calcium molybdate and calcium vanadate, solutions CS1, CS2 and CSV1 were used for the sodium system and CK1, CK2 and CKV1 for the potassium system.

Table 4-1: Starting composition of the solutions used in the precipitation experiments together with the pH of solution after the calcium oxide was dosed, the residence time and the dosage of calcium oxide.

	Composition start solution [w%]					Res. Time	
Solution	$NaNO_3$	Na_2SO_4	Na_2MoO_4	$NaVO_3$	pH	[min]	CaO dosage
CS1							
CS2							
CSV1							
CSV2							
CSV3							
	KNO_3	K_2SO_4	Na_2MoO_4	$NaVO_3$	pH	Res. Time	CaO dosage
CK1							
CK2							
CKV1							
CKV2							

Experiments CS1, CSV1, CK1 and CKV1 were conducted for an equimolar dosage and experiments CS2 and CK2 for a double molar dosage of calcium oxide. In all experiments the pH was varied from not neutralized, #, to a pH of #. For each pH (#) a new starting solution was used and each was dosed with the desired amount of calcium oxide. So experiment CS1, for example, was conducted with 4 separate solutions, all of the same starting composition and dosed with the same amount of calcium oxide, but kept at a different pH.

At the end of each experiment samples of the solution were taken and were filtrated in a glass filter. A solid sample was taken by filtrating the remaining mixture after which the solid residue could be collected from the filter.

The calcium oxide dosage was calculated with the following reaction equations:

$$2CaO + Na_2MoO_4 + 2NaVO_3 \longrightarrow CaMoO_4 + Ca(VO_3)_2 + 4NaOH \tag{4-1}$$

$$2CaO + K_2MoO_4 + 2KVO_3 \longrightarrow CaMoO_4 + Ca(VO_3)_2 + 4KOH \tag{4-2}$$

$$m_{CaO} = \left(\frac{w_{Na_2MoO_4}}{MW_{Na_2MoO_4}} + \frac{1}{2}\frac{w_{NaVO_3}}{MW_{NaVO_3}}\right) MW_{CaO} \tag{4-3}$$

With w the concentration of the corresponding compound and MW the molecular weight. The equation for the dosage of calcium oxide for the potassium system is similar to that of the sodium system (4-3) as only the compound concentrations and molecular weights should be changed to those of the potassium compounds.

4-2-2 Effect of residence time

The effect of residence time on the precipitation of calcium molybdate and calcium vanadate was studied with solutions CSV2, CSV3 and CVK2.
In experiment CSV2 an equimolar amount of calcium oxide was added to the solution, the pH of the solution was not neutralized with nitric acid (so pH was around #) and the was left to stir for # minutes. In experiment CSV3 again an equimolar amount of calcium oxide was added to the solution and this time nitric acid was added to reduce the solution pH to around #. This solution was also left to stir for # minutes. Finally, in experiment CKV2 an equimolar amount of calcium oxide was added to the solution and initially the solution was not neutralized. After # minutes of stirring, the nitric acid was added to reach a solution pH of around # and the solution was left to stir for another # min.
Samples of the solutions were taken every # minutes for experiments CSV1 and CSV2 and every # minutes for experiment CKV2.

4-3 Results and discussion

In figure 4-3 the concentration of molybdate, vanadate and calcium in the solutions of experiments CS1 and CS2 are shown. In figure 4-4 this is shown for experiments CK1 and CK2.
The molybdate concentration in the sodium system decreased with about # ppm after the calcium oxide was dosed and lowering the pH reduced this content further. At a pH of #, however, the molybdate concentration increased again. The dosage of calcium oxide did not seem to have much effect on the molybdate concentration. The dosage has an effect on the calcium concentration, however. This is about triple that of the of the equimolar dosage and increased with decreasing pH, which was as expected for calcium.
The molybdate concentration in the potassium system is hardly reduced by the calcium oxide when compared to the sodium system. Dosage of calcium oxide again did not have a significant effect on the molybdate concentration. As was with the sodium system, the calcium concentration is affected by the calcium dosage and increased with decreasing pH.

Figure 4-3: Experiments CS1 and CS2: Concentration in ppm of molybdate, vanadate and calcium in the solution plotted against the pH of the solution. Also two different dosages of CaO were used: equimolar amount and double molar amount with respect to the molybdate and vanadate concentration of the solution.

In figures 4-5 and 4-6 the concentration of molybdate, vanadate and calcium in the solutions of experiment CSV1 and CKV1, respectively, are shown.
For experiment CSV1 the same trend is shown as for experiments CS1 and CS2: the

Figure 4-4: Experiments CK1 and CK2: Concentration in ppm of molybdate, vanadate and calcium in the solution plotted against the pH of the solution. Also two different dosages of CaO were used: equimolar amount and double molar amount with respect to the molybdate and vanadate concentration of the solution.

molybdate concentration decreased with about # ppm after dosing the calcium oxide. A lower pH resulted in a lower molybdate concentration, however, at a pH of # this concentration increased a little. The vanadate concentration shows a similar trend as that of the molybdate and decreases with decreasing pH. At the minimum, the molybdate was reduced to below # ppm and vanadate to below # ppm.
The nice results with experiment CSV1 were not obtained with the experiment CKV1: Again the molybdate concentration is hardly reduced by the calcium oxide, regardless of the pH. The concentration fluctuates around that of the starting composition. The vanadate concentration was decreased with about # ppm and found a minimum at a pH of #, after which it increased again for lower pH. A large part of the calcium oxide seems to dissolve, even at a pH of #, as the calcium concentration in the solution increased.

Figure 4-5: Experiment CSV1: Concentration in ppm of molybdate, vanadate and calcium in the solution plotted against the pH of the solution.

Figure 4-6: Experiment CKV1: Concentration in ppm of molybdate, vanadate and calcium in the solution plotted against the pH of the solution.

In figures 4-7 and 4-8 the composition of the precipitated solids from experiment CSV1 and CKV1 are shown versus the pH. For experiment CSV1 the decrease in molybdate and vanadate content in the solution corresponds directly to the increase of these components in the precipitates. The amount of sulfate that precipitates is minimal.
For experiment CKV1, however, it can be observed that mostly calcium sulfate has precipitated. For the experiments with a pH of # and # insufficient solids formed and no sample could be taken.

Figure 4-7: Experiment CSV1: Composition in w% of the formed solid phase during the precipitation process

Figure 4-8: Experiment CKV1: Composition in w% of the formed solid phase during the precipitation process. For pH # and # insufficient solids had formed.

In figures 4-9, 4-10 and 4-11 the results of experiments CSV2, CSV3 and CKV2 are shown respectively. At t=0 the calcium oxide was dosed. The results from experiment

CSV2 show no further decrease, besides the initial # ppm reduction, in the molybdate concentration over time for a solution that was not neutralized and therefore had a pH of around #. This result corresponds to those in figures 4-5 and 4-3 as there a decrease of about # ppm was observed at a pH of #. Also a dip can be observed at # min. This is probably an error resulting from sampling or diluting for ICP analysis as this dip can be observed for all three components.
The results from experiment CSV3 show the desired results: After # minutes the pH of the solution was decreased to # and from that moment a step decrease in both molybdate and vanadate concentration can be observed. After # minutes the concentration of these components increase a little as the pH was lowered too much, to around # - #.
The results form experiment CKV2 show again little response to the calcium oxide. The calcium concentration increases over time and after # minutes, when the pH was lowered to #, increases with a step to about # ppm. Both the molybdate and vanadate fluctuate around their initial concentration.

Figure 4-9: Experiment CSV2: Concentration in ppm of molybdate, vanadate and calcium in the solution plotted against the residence time. In this experiment the pH was not reduced by the addition of nitric acid.

Figure 4-10: Experiment CSV3: Concentration in ppm of molybdate, vanadate and calcium in the solution plotted against the residence time. In this experiment the pH was reduced to about # by the addition of nitric acid.

Figure 4-11: Experiment CKV2: Concentration in ppm of molybdate, vanadate and calcium in the solution plotted against the residence time. In this experiment the pH was initially not reduced, but at t = # min. the pH was reduced to about # by the addition of nitric acid.

4-3-1 Mean particle size

In order to determine the settling velocity, a mean particle size of the formed calcium components has to be determined. In figures 4-12 and 4-13 formed crystals during experiment CSN and CK, respectively, can be observed. The photos were taken from the solids in solution.
In figure 4-12, the left picture was taken after # minutes, while the right one was taken after # min. The mean particle size was determined by observation and measuring the approximate particle diameters in the figures. The mean particle size of the particles

in the two figures is given in table 4-2. It can be observed that the mean particle size changed less than #% over # minutes, indicating slow crystallization kinetics

Table 4-2: Mean particle size for experiment CSN

time [min.]	mean particle size [μm]

In figure 4-13 most solids are calcium sulfate, indicated by their needle shaped crystals [42]. The black somewhat spherical particles are most probably calcium vanadate and calcium molybdate. Finding a mean particle size for the precipitates in the potassium system is at the moment irrelevant, as first a solution has to be found for the selectivity towards calcium sulfate precipitation instead of calcium molybdate and calcium vanadate.

Figure 4-12: Experiment CSN - image of the formed particles as viewed under the microscope. Left an image taken after # min. and right after # min.

Figure 4-13: Experiment CK - image of the formed particles as viewed under the microscope. Left an image taken after # min. and right after # min.

4-4 Conclusions

For the sodium system, both molybdate and vanadate were successfully precipitated out of the solution with an equimolar dosage of calcium oxide. Starting with # ppm or # ppm of molybdate in solution resulted in a final concentration of below # ppm of molybdate in the solution. The vanadate concentration in solution was reduced to below # ppm. Precipitation of calcium sulfate was kept to a minimum as the formed precipitate consisted of only #% sulfate. The best results were obtained at a solution pH of #, decreasing the pH further resulted in a higher molybdate and vanadate concentration in the solution. Studying the precipitation process over time showed a steep decline in molybdate and vanadate concentration during the first # minutes after the calcium oxide was dosed after which a minimum concentration was found at # minutes. With a mean particle size of about # μm, a settling device can be designed for the separation of the solid phase from the solution.

For the potassium system, precipitation of molybdate and vanadate with calcium oxide was unsuccessful. The molybdate and vanadate concentrations were hardly reduced and instead a part of the calcium oxide dissolved or precipitated as calcium sulfate as the formed solid phase consisted of more than #% of sulfate. A minimum concentration of molybdate and vanadate was found at a pH of #. Residence time did not seem to have much influence on the precipitation process.

4-4-1 Implications for the process design

For the sodium system a precipitation vessel needs to be designed with a residence time of about # to # minutes. In order to keep the pH of the solution at #, nitric acid needs to be added according to the solution feed. With the found mean particle size a settling device can be designed.

For the potassium system another method needs to be found to reduce the molybdate and vanadate content in the solution. Another option is to first reduce the sulfate content and subsequently try to precipitate the molybdate and vanadate with calcium oxide.

Chapter 5

Process flow model for the Salt Sludge Separation process

For confidentiality purposes, most results have been left out of this report

In this chapter the experimental results from the EFC experiments and the calcium precipitation experiments are used in the development of a steady state process flow model that will help with the development of an economical process design for the salt sludge separation process.

Rejection of potassium hydroxide as neutralizing agent

One conclusion that can be drawn from the experiments is that with the neutralization with potassium hydroxide, the separation of molybdate and vanadate from the system becomes very difficult. Other disadvantages are the slow crystallization kinetics and excessive scaling encountered with the potassium salts. These drawbacks of the potassium system will translate to higher residence times and therefore larger vessels and at the same time the excessive scaling will call for more costly scraping equipment. Overall, this will result in much higher operating costs than for the sodium system. The decisive factor for the rejection of the potassium hydroxide base is the costs for raw materials versus the income from the produced salt products: Potassium hydroxide is a costly raw material and only the production of potassium salts of a high grade will give a profitable process. However, as the calcium precipitation experiments have shown, the molybdate and vanadate content in the potassium nitrate product could hardly be reduced, resulting in a potassium nitrate product that will not meet the required purity standards.

Therefore, on preliminary basis, the system with potassium hydroxide is rejected as option for the salt sludge separation process.

Figure 5-1: Block diagram of the salt sludge separation process.

In figure 5-1 the block diagrams of the EFC process and the calcium precipitation procces are connected in series, resulting in the following process: The feed stream, coming from the HyVent Metal Recovery process, is fed to a buffer vessel were it is neutralized with NaOH and the resulting stream is processed in the EFC crystallizer. Here the entering stream is reduced in water (ice) and sodium sulfate (as sodium sulfate decahydrate) concentration and the resulting concentration sodium nitrate stream leaves the crystallizer as bleed stream. The formed ice leaves the crystallizer over the top with a certain amount of mother liquor and this slurry is separated on a solid/liquid separator into an ice product and a liquid filtrate. In a similar manner the sodium sulfate decahydrate crystals leave via the bottom of the crystallizer and on a different solid/liquid separator this slurry is separated into the sodium sulfate decahydrate product and a liquid filtrate. The filtrates are recycled to the buffer vessel. Although some of the sodium molybdate and sodium vanadate leave the system via the ice and sodium sulfate decahydrate product, the majority is still present in the concentrated sodium nitrate stream. Therefore, the bleed stream is fed to a precipitation vessel where calcium oxide is dosed to the stream and the molybdate and vanadate precipitate as calcium molybdate and calcium vanadate. These impurities are separated from the concentration sodium nitrate stream in a gravitational settler and the resulting stream is the sodium nitrate product.
The reason that the precipitation procces is placed after the EFC process is that in this configuration no calcium ends up in the ice product. As the water is recycled to the HyVent metal recovery process, presence of calcium in the recycle water would give rise to scaling problems. In the current process configuration, calcium only leaves the system in small amounts with the concentrated sodium nitrate product and the majority in the form of precipitates of molybdate, vanadate and sulfate.

5-1 Development of process model

5-1-1 Assumptions

The following assumptions are applied for the model development:

- Steady state operation.
- All streams are homogeneously mixed.

- no melting of ice on the solid/liquid separator of the ice product, pipes or other equipment.
- no dissolution of sodium sulfate decahydrate on the solid/liquid separation of the sodium sulfate salt product, pipes or other equipment.
- Solid fraction in the EFC crystallizer, ice slurry and sodium sulfate decahydrate slurry is #% [35] [46].
- Based on the EFC batch experience, the mother liquor content in the ice and sodium sulfate salt products is # w%
- Based on the calcium precipitation experiments, the dissolved calcium concentration in the sodium nitrate product stream is about # ppm.
- Based on the calcium precipitation experiments, the sodium molybdate concentration is reduced with #% and the sodium vanadate concentration is reduced with #% by the precipitation with calcium.
- The solid fraction in the filtrate streams, process stream and bleed stream is zero.
- A #% heat loss is assumed for the EFC crystallizer, a temperature increase of # $^{\circ}C$ is assumed for the solid/liquid separators.
- Pipes and other equipment are considered perfectly insulated and therefore the heat transfer to the environment is negligible.

5-1-2 Model decomposition and input parameters

The process can be divided into five components with the following input and output:

1. The EFC crystallizer.
2. The solid/liquid separator for the ice product.
3. The solid/liquid separator for the sodium sulfate product.
4. The buffer/mixer vessel for the feed stream and filtrate recycle streams.
5. The calcium precipitation vessel and settler.

The following input parameters are used in the model:

- $\dot{m}_{in}$, the mass flow of the incoming stream from the HyVent metal recovery process.
- $w_{in,i}$, the mass fraction of the component i of the incoming stream.

- T_{in}, the temperature of the incoming stream
- pH_{in}, the pH of the incoming stream
- w_{NaOH}, the mass fraction/purity of the NaOH base.
- T_{NaOH}, the temperature of the NaOH base.
- T_{cr}, the operating temperature of the EFC crystallizer.
- w_{CaO}, the mass fraction/purity of the calcium oxide used in the precipitation vessel.
- w_{HNO_3},the mass fraction/purity of the nitric acid used in the precipitation vessel.

5-1-3 Operating region of the EFC crystallizer

In figure 5-2 the ternary phase diagram of sodium nitrate, sodium sulfate and water is shown. The path of operation is represented by the red line, starting at the feed composition, indicated by the red circle. It can be observed that the crystallization process in the EFC crystallizer can be split up into three parts: The feed composition is in the area where sodium sulfate is the first compound to crystallize (as decahydrate) and therefore, first a cooling crystallization process will take place until the eutectic line of sodium sulfate an water is reached (the blue line). From that point on, an EFC process takes place, until the operating temperature in the crystallizer or the ternary eutectic point of sodium nitrate, sodium sulfate and water is reached. Further cooling at the ternary eutectic point causes also the crystallization of sodium nitrate. For modeling purposes it is important to distinguish these three crystallization processes, however, take note that during continuous steady state operation, these crystallization processes take place simultaneously and a constant flow of both ice and sodium sulfate salt is produced.

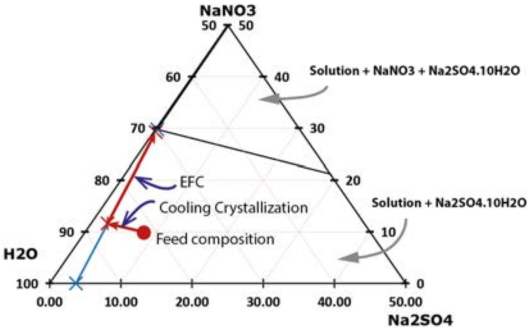

Figure 5-2: Ternar phase diagram of the $NaNO_3$,Na_2SO_4 and water system. The eutectic line of $Na_2SO_4 \cdot 10H_2O$ and ice is indicated by the blue line, the feed composition is indicated by the red circle and the crystallization path is represented by the red line.

The operating temperature of the EFC crystallizer is an important input parameter, as on one hand this determines the composition of the mother liquor leaving the crystallizer while on the other hand determines to what temperature the feed stream needs to be cooled.

For the modeling of the crystallization process, the composition and temperature of some points in the phase diagram are of importance:

- Feed composition point.
- Binary eutectic point of water and sodium sulfate.
- Ternary eutectic point of sodium nitrate, sodium sulfate and water.
- Point on the eutectic line of water and sodium sulfate where the cooling crystallization process ends and EFC process starts.

The intersection of the cooling crystallization path and the eutectic line of water and sodium sulfate, is the only point that is unknown in terms of solution composition and temperature and can be determined with the following equations.

The slope of the eutectic line of water and sodium sulfate and the slope of the line representing the cooling crystallization process:

$$\text{slope}_{EFC} = \frac{y_{tern}}{x_{tern} - x_{bin}} \tag{5-1}$$

$$\text{slope}_{CC} = \frac{-y_f}{x_{hydr} - x_f} \tag{5-2}$$

With y the y-coordinate in the phase diagram (= sodium nitrate concentration) and x the x-coordinate in the phase diagram (=0.5 · sodium nitrate composition + sodium sulfate composition). The subscripts *tern*, *bin*, *f* and *hydr* represent the ternary, binary, feed and the sodium sulfate composition of the decahydrate salt.

With the slope of the two lines known, the x and y coordinates of the intersection point of the two lines can be determined:

$$x_{cc} = \frac{-\text{slope}_{CC} \cdot x_f + y_f + \text{slope}_{EFC} \cdot x_{bin}}{\text{slope}_{EFC} - \text{slope}_{CC}} \tag{5-3}$$

$$y_{cc} = \text{slope}_{EFC} \cdot x_{cc} - \text{slope}_{EFC} \cdot x_{bin} \tag{5-4}$$

In turn, these coordinates can be translated to the sodium nitrate (subscript N) and sodium sulfate (subscript S) mass fraction of the solution at the intersection point:

$$w_{cc,N} = y_{cc} \tag{5-5}$$

$$w_{cc,S} = x_{cc} - 0.5 \cdot y_{cc} \tag{5-6}$$

With the composition at the intersection, the temperature at this point can be interpolated from the temperature and composition of the binary and ternary eutectic points:

$$T_{cc} = \frac{T_{bin} - T_{tern}}{w_{bin,S} - w_{tern,S}} \cdot (w_{cc,S} - w_{tern,S}) + T_{tern} \tag{5-7}$$

Freeze concentration

As the feed composition is an input parameter, the user model can also specify a feed composition that is in the area where water is the component the crystallizes first. In this case the solution concentrates by the crystallization of ice, until the eutectic line of water and sodium sulfate is reached and EFC of ice and sodium sulfate decahydrate commences.
In order to determine the crystallization path of the freeze concentration in the phase diagram, a similar approach can be used as for the cooling crystallization process. The slope of the freeze concentration line is determined by the feed composition and the composition of the ice that has formed, which is 100% water. The intersection with the eutectic line determines the composition of the solution at the end of the freeze conceration process as well as the temperature at that point.

5-1-4 Mass balance equations

For the different components specified under 'Model decomposition' mass balances can be formulated and solved for the unknown variables. In the equations w represents the mass fraction, $\dot{m}$ mass flow, MW_i molecular weight of component i. The subscripts N, S, S_{10}, M and V represent the components $NaNO_3$, Na_2SO_4, $Na_2SO_4 \cdot 10H_2O$, Na_2MoO_4, $NaVO_3$ respectively. when referred to component i, the equation can be used for sodium nitrate, sodium sulfate, sodium molybdate and sodium vanadate.

Thermal properties of the solution and components used in the model

Thermal properties of the aqueous solutions of sodium nitrate and sodium sulfate are provided in appendix C. The influence of the sodium molybdate and sodium vanadate content in de solution and solids is neglected, as the concentrations are small compared to the sodium nitrate concentration.
For the viscosity and density, the mean values of the sodium nitrate solution and sodium sulfate solution are used, e.g:

$$\rho_{\text{solution}} = \frac{\rho_{aq,N} + \rho_{aq,S}}{2} \tag{5-8}$$

The heat capacity of the solution with varying concentration is determined with the partial molar heat capacities of sodium nitrate solution and sodium sulfate solution:

$$Cp_{\text{solution}} = Cp_{aq,N} \cdot X_N + Cp_{aq,S} \cdot X_S + Cp_{aq,H_2O} \cdot X_{H_2O} \tag{5-9}$$

The feed

The feed stream consists of the incoming stream from the HyVent metal recovery process, which is neutralized with sodium hydroxide. The flow of sodium hydroxide depends on the mass flow and pH of the incoming stream:

$$\dot{m}_{base} = \frac{\dot{m}_{in} \cdot 10^{(pH_{in})}}{\rho_{in}} \cdot \frac{MW_{NaOH}}{MW_{NO_3} \cdot w_{NaOH}} \tag{5-10}$$

The feed mass flow and concentration of component i is then given by:

$$\dot{m}_f = \dot{m}_{in} + \dot{m}_{base} \tag{5-11}$$

$$w_{f,i} = \frac{\dot{m}_{in} \cdot w_{in,i} + \dot{m}_{base} \cdot w_{base,i}}{\dot{m}_f} \tag{5-12}$$

EFC crystallizer

The operating temperature of the EFC crystallizer determines the composition of the mother liquor that leaves the crystallizer. As the operating temperature refers to a composition on the eutectic line of sodium sulfate and water, the mass fractions of sodium nitrate and sodium sulfate at this temperature can be determined by interpolating the operating temperature with the temperature and compositions of the binary and ternary eutectic points of (sodium nitrate), sodium sulfate and water:

$$w_{cr,N} = \frac{T_{cr} - (-17.59)}{(-1.16) - (-17.59)} \cdot (0 - 29.75) + 29.75 \tag{5-13}$$

$$w_{cr,S} = \frac{T_{cr} - (-17.59)}{(-1.16) - (-17.59)} \cdot (3.67 - 0.23) + 0.23 \tag{5-14}$$

As was mentioned before, the crystallization process in the EFC crystallizer can be split into three parts:

1. **Cooling crystallization of $\mathbf{Na_2SO_4 \cdot 10H_2O}$:** The concentration factor of the cooling crystallization process CF_{cc} can be used to determine the concentration of Na_2MoO_4 and $NaVO_3$ at the end of the cooling crystallization process and start

of EFC process. The concentration factor is defined as:

$$CF_{cc} = \frac{w_{cc,N}}{w_{f,N}} \tag{5-15}$$

As all sodium sulfate stays in solution, the amount of solution that is left at the end of the cooling crystallization process is then given by:

$$\dot{m}_{cc} = \frac{\dot{m}_f \cdot w_{f,N}}{w_{cc,N}} \tag{5-16}$$

A mass reduction factor of the solution can be introduced, which is used to determine the amount of $Na_2SO_4 \cdot 10H_2O$ that is formed during the cooling crystallization process:

$$MR_{cc} = 1 - (\frac{1}{CF_{cc}}) \tag{5-17}$$

$$\dot{m}_{cc,S_{10}} = \dot{m}_f \cdot MR_{cc} \tag{5-18}$$

The concentration of sodium molybdate and sodium vanadate in the solution at the end of the cooling crystallization process can be determined with:

$$w_{cc,i} = w_{f,i} \cdot CF_{cc} \tag{5-19}$$

2. **EFC of ice and $\mathbf{Na_2SO_4 \cdot 10H_2O}$:** For the EFC process the concentration factor can again be determined from the difference in sodium nitrate mass fraction and the corresponding mass reduction factor can be determined.

$$CF_{EFC} = \frac{w_{cr,N}}{w_{cc,N}} \tag{5-20}$$

$$MR_{EFC} = 1 - (\frac{1}{CF_{EFC}}) \tag{5-21}$$

The mass fraction of sodium molybdate and sodium vanadate of the mother liquor leaving the crystallizer is given by:

$$w_{cr,i} = w_{cc,i} \cdot CF_{EFC} \tag{5-22}$$

The amount of solids formed at the end of the EFC process is formulated as the mass reduction of the solution at the start of the EFC process, $\dot{m}_{cc}$. The ratio to which these solids are $Na_2SO_4 \cdot 10H_2O$ and ice can be determined with the composition of the solution at the end of the EFC process:

$$\dot{m}_{EFC,S_{10}} = \dot{m}_{cc} \cdot MR_{EFC} \cdot w_{cr,S} \frac{MW_{S_{10}}}{MW_S} \tag{5-23}$$

$$\dot{m}_{EFC,ice} = \dot{m}_{cc} \cdot MR_{EFC} - \dot{m}_{EFC,S_{10}} \tag{5-24}$$

3. **EFC of ice, $NaNO_3$ and $Na_2SO_4 \cdot 10H_2O$:** For the EFC process at the ternary eutectic point a concentration factor has to be determined with the maximum allowable sodium molybdate concentration in the bleed stream of the crystallizer $w_{X,M}$.

$$CF_{TERN} = \frac{w_{X,M}}{w_{cr,M}} \tag{5-25}$$

$$MR_{TERN} = 1 - (\frac{1}{CF_{TERN}}) \tag{5-26}$$

The mass fraction of sodium molybdate and sodium vanadate of the mother liquor leaving the crystallizer is given by:

$$w_{cr,i} = w_{cr,i} \cdot CF_{TERN} \tag{5-27}$$

The amount of solids formed at the end of the EFC process is formulated as the mass reduction of the solution at the start of the EFC process, $\dot{m}_{cc}$. The ratio to which these solids are $Na_2SO_4 \cdot 10H_2O$ and ice can be determined with the composition of the solution at the end of the EFC process:

$$\dot{m}_{TERN,S_{10}} = \dot{m}_{efc} \cdot MR_{TERN} \cdot w_{cr,S} \frac{MW_{S_{10}}}{MW_S} \tag{5-28}$$

$$\dot{m}_{TERN,N} = \dot{m}_{EFC} \cdot MR_{TERN} \cdot w_{cr,N} \tag{5-29}$$

$$\dot{m}_{TERN,ice} = \dot{m}_{EFC} \cdot MR_{EFC} - \dot{m}_{TERN,N} - \dot{m}_{EFC,S_{10}} \tag{5-30}$$

Finally, the total amount of $Na_2SO_4 \cdot 10H_2O$, $NaNO_3$ and ice are given by:

$$\dot{m}_{S_{10}} = \dot{m}_{EFC,S_{10}} + \dot{m}_{EFC,S_{10}} + \dot{m}_{TERN,S_{10}} \tag{5-31}$$

$$\dot{m}_{ice} = \dot{m}_{EFC,ice} + \dot{m}_{TERN,ice} \tag{5-32}$$

$$\dot{m}_N = \dot{m}_{TERN,N} \tag{5-33}$$

Solid/liquid separator for ice product

The ice product leaves the crystallizer as a slurry and is separated into mother liquor and ice on a vacuum belt filter. The mass flow of the ice slurry can be determined the solid fraction in the slurry, which is #%:

$$\dot{m}_{sl,ice} = \frac{\dot{m}_{ice}}{\epsilon_{ice}} \tag{5-34}$$

The total composition (solids + mother liquor) of the ice slurry can be calculated with:

$$w_{sl,ice,i} = \frac{\dot{m}_{sl,ice} \cdot (1 - \epsilon_{ice}) \cdot w_{cr,i}}{\dot{m}_{sl,ice}} \tag{5-35}$$

As there is no melting of ice on the filter the ice filtrate has the composition of the mother liquor in the crystallizer:

$$w_{fil,ice,i} = w_{cr,i} \tag{5-36}$$

Another assumption specifies that the mother liquor content in the ice product is #%. The ice product flow and composition is then given by:

$$\dot{m}_{P,ice} = \dot{m}_{ice} \cdot \tag{5-37}$$

$$w_{P,ice,i} = \frac{\dot{m}_{ice} \cdot 0.05 \cdot w_{cr,i}}{\dot{m}_{P,ice}} \tag{5-38}$$

Finally, the mass balance of the ice filter can be used to determine the ice filtrate flow:

$$\dot{m}_{fil,ice} = \dot{m}_{sl,ice} - \dot{m}_{P,ice} \tag{5-39}$$

Solid/liquid separator for sodium sulfate product

In a similar way the mass balance of the salt filter is solved: The salt slurry consists of #% solids.

$$\dot{m}_{slS_{10}} = \frac{\dot{m}_{S_{10}}}{\epsilon_{S_{10}}} \tag{5-40}$$

$$w_{slS_{10},i} = \frac{\dot{m}_{sl,S_{10}} \cdot (1 - \epsilon_{S_{10}}) \cdot w_{cr,i}}{\dot{m}_{sl,S_{10}}} \tag{5-41}$$

As there is no dissolution of $Na_2SO_4 \cdot 10H_2O$ on the filter the salt filtrate has the composition of the mother liquor in the crystallizer:

$$w_{filS_{10},i} = w_{cr,i} \tag{5-42}$$

The $Na_2SO_4 \cdot 10H_2O$ product also contains #% mother liquor. The sodium sulfate product flow and composition is then given by:

$$\dot{m}_{PS_{10}} = \dot{m}_{S_{10}} \cdot \tag{5-43}$$

$$w_{PS_{10},i} = \frac{\dot{m}_{S_{10}} \cdot \cdot w_{cr,i}}{\dot{m}_{PS_{10}}} \tag{5-44}$$

Finally, the salt filtrate flow can be obtained by solving the mass balance of the salt filter:

$$\dot{m}_{filS_{10}} = \dot{m}_{slS_{10}} - \dot{m}_{PS_{10}} \tag{5-45}$$

Buffer vessel

Both the filtrate streams are recycled to the buffer vessel. The feed enters the buffer vessel and a process stream leaves the vessel to the crystallizer. This process stream is the sum of the incoming streams and the composition can be determined with the component balance:

$$\dot{m}_{pr} = \dot{m}_f + \dot{m}_{fil,S_{10}} + \dot{m}_{fil,ice} \tag{5-46}$$

$$w_{pr,i} = \frac{\dot{m}_f \cdot w_{f,i} + \dot{m}_{fil,S_{10}} \cdot w_{fil,S_{10},i} + \dot{m}_{fil,ice} \cdot w_{fil,ice,i}}{\dot{m}_{pr}} \tag{5-47}$$

Precipitation vessel and settler

The bleed stream that leaves the EFC crystallizer is fed to the precipitation vessel. The flow of the bleed stream is the overall mass balance of the crystallizer, buffer vessel and both the filters and has a composition of that of the mother liquor in the crystallizer:

$$\dot{m}_{bl} = \dot{m}_f - \dot{m}_{P,ice} - \dot{m}_{P,S_{10}} \tag{5-48}$$

$$w_{bl,i} = w_{cr,i} \tag{5-49}$$

The amount of calcium oxide that is required for the precipitation of calcium molybdate and calcium vanadate from the incoming bleed stream can be determined with the reaction equation:

$$2CaO + Na_2MoO_4 + 2NaVO_3 + 2H_2O \rightarrow CaMoO_4 + Ca(VO_3)_2 + 4NaOH \tag{5-50}$$

The flow of calcium oxide is then given by:

$$\dot{m}_{CaO} = \frac{\left(\frac{\dot{m}_{bl} \cdot w_{bl,M}}{MW_M} + \frac{1}{2}\frac{\dot{m}_{bl} \cdot w_{bl,V}}{MW_V}\right) \cdot MW_{CaO} \cdot e_{CaO}}{w_{CaO}} \tag{5-51}$$

The pH in the precipitation vessel is regulated to maintain a pH of #. The amount of nitric acid required to do this can be determined with the following equations:

$$\dot{n}_{OH} = \frac{\dot{m}_{CaO} \cdot w_{CaO}}{\dot{m}_{CaO} + \dot{m}_{bl}} \cdot \frac{1}{MW_{CaO}} \cdot \rho_{bl} \tag{5-52}$$

$$\dot{m}_{HNO_3} = \frac{\left(\frac{\dot{n}_{OH} - 10^{-(14-10)}}{\rho_{bl}} \cdot MW_{HNO_3}\right) \cdot \dot{m}_{bl}}{w_{HNO_3}} \tag{5-53}$$

The flow and composition of the stream (suspension) leaving the precipitation vessel to the settler can be determined with the mass and component balance of the precipitation vessel:

$$\dot{m}_{\text{settler}} = \dot{m}_{bl} + \dot{m}_{CaO} + \dot{m}_{HNO_3} \tag{5-54}$$

$$w_{\text{settler},i} = \frac{\dot{m}_{bl} \cdot w_{bl,i}}{\dot{m}_{\text{settler}}} \tag{5-55}$$

As nitric acid is added in the precipitation vessel, the concentration of sodium nitrate in the stream leaving the precipitation vessel is given by:

$$w_{\text{settler},N} = \frac{\dot{m}_{bl} \cdot w_{bl,N} + \dot{m}_{HNO_3} \cdot w_{HNO_3} \cdot \dfrac{MW_N}{MW_{HNO_3}}}{\dot{m}_{\text{settler}}} \tag{5-56}$$

In a similar way, the concentration of calcium in the stream leaving the precipitation vessel is given by:

$$w_{\text{settler},Ca} = \frac{\dot{m}_{CaO} \cdot w_{CaO} \cdot \dfrac{MW_{Ca}}{MW_{CaO}}}{\dot{m}_{\text{settler}}} \tag{5-57}$$

The concentrated sodium nitrate product stream can be obtained from the component balance of sodium nitrate, as no nitrate leaves the system as precipitate of calcium:

$$\dot{m}_{P,N} = \frac{\dot{m}_{\text{settler}} \cdot w_{\text{settler},N}}{w_{PN,N}} \tag{5-58}$$

The amount of precipitated solids is then given by:

$$\dot{m}_{\text{precip}} = \dot{m}_{\text{settler}} - \dot{m}_{P,N} \tag{5-59}$$

As the assumptions specify that the sodium molybdate and sodium vanadate concentrations are reduced with #% and #% respectively, the concentrations of these components in the sodium nitrate product stream are given by:

$$w_{PN,M} = () \cdot w_{\text{settler},M} \tag{5-60}$$

$$w_{PN,V} = () \cdot w_{\text{settler},V} \tag{5-61}$$

The amount of calcium molybdate and calcium vanadate that have precipitated can be determined with the component balances of the settler:

$$\dot{m}_{CaMoO_4} = (\dot{m}_{\text{settler}} \cdot w_{\text{settler},M} - \dot{m}_{P,N} \cdot w_{PN,M}) \cdot \frac{MW_{CaMoO_4}}{MW_M} \tag{5-62}$$

The amount of moles of calcium vanadate are half that of the sodium vanadate.

$$\dot{m}_{Ca(VO_3)_2} = (\dot{m}_{\text{settler}} \cdot w_{\text{settler},M} - \dot{m}_{P,N} \cdot w_{PN,M}) \cdot \frac{MW_{Ca(VO_3)_2}}{2 \cdot MW_V} \tag{5-63}$$

The amount of calcium sulfate that precipitates is given by the remaining calcium that has not precipitated as calcium molybdate or calcium vanadate or the calcium that has left the system via the sodium nitrate product stream:

$$\dot{m}_{CaSO_4} = \left(\frac{\dot{m}_{CaO}}{MW_{CaO}} - \frac{\dot{m}_{P,N} \cdot w_{PN,Ca}}{MW_{Ca}} - \frac{\dot{m}_{CaMoO_4}}{MW_{CaMoO_4}} - \frac{\dot{m}_{Ca(VO_3)_2}}{MW_{Ca(VO_3)_2}}\right) \cdot MW_{CaSO_4} \tag{5-64}$$

The composition of the calcium precipitate product is given by the following equation, with i components calcium molybdate, calcium vanadate and calcium sulfate.

$$w_{\text{precip},i} = \frac{\dot{m}_{Ca,i}}{\dot{m}_{CaMoO_4} + \dot{m}_{Ca(VO3)_2} + \dot{m}_{CaSO_4}} \tag{5-65}$$

Finally, the sodium sulfate concentration in the sodium nitrate product stream is given by:

$$w_{PN,S} = \frac{\left(\dot{m}_{\text{settler}} \cdot w_{\text{settler},S} - \dot{m}_{\text{precip}} \cdot w_{\text{precip},CaSO_4} \cdot \dfrac{MW_S}{MW_{CaSO_4}}\right)}{\dot{m}_{P,N}} \tag{5-66}$$

Product purity

The product purities of the three product streams are given by the following equations. The purity of the sodium nitrate stream is that of the dry sodium nitrate product, so not as concentrated solution.

$$P_{ice} = (1 - w_{ice,N} - w_{ice,S} - w_{ice,M} - w_{ice,V}) \cdot 100\% \tag{5-67}$$

$$P_N = \left(\frac{w_{PN,N}}{w_{PN,N} + w_{PN,S} + w_{PN,M} + w_{PN,V} + w_{PN,Ca}}\right) \cdot 100\% \tag{5-68}$$

$$P_{S_{10}} = \left(\frac{w_{PS_{10},S_{10}}}{w_{PS_{10},N} + w_{PS_{10},S_{10}} + w_{PS_{10},M} + w_{PS_{10},V}}\right) \cdot 100\% \tag{5-69}$$

5-1-5 Energy balance equations

$$T_{sl,ice} = T_{sl,S_{10}} = T_{bl} = T_{cr} \tag{5-70}$$

$$T_{fil,ice} = T_{fil,S_{10}} = T_{sl,ice} + \Delta T_{\text{loss}} \tag{5-71}$$

$$T_{P,ice} = T_{P,S_{10}} = T_{sl,ice} + \Delta T_{\text{loss}} \tag{5-72}$$

$$T_{pr} = \frac{\dot{m}_f \cdot cp_f \cdot T_f + \dot{m}_{fil,ice} \cdot cp_{fil,ice} \cdot T_{fil,ice} + \dot{m}_{fil,S_{10}} \cdot cp_{fil,S_{10}} \cdot T_{fil,S_{10}}}{\dot{m}_{pr} \cdot cp_{pr}} \tag{5-73}$$

$$T_{\text{settler}} = T_{P,N} = 20°C \tag{5-74}$$

Similar as for the mass balance of the ECF crystallizer, the energy balance of the crystallizer can be split in multiple components:

1. Cooling of the solution for the cooling crystallization of $Na_2SO_4 \cdot 10H_2O$.

$$\dot{Q}_{cc,sol} = \dot{m}_{pr} \cdot Cp_{sol} \cdot (T_{pr} - T_{cc}) \tag{5-75}$$

2. Cooling of the formed $Na_2SO_4 \cdot 10H_2O$ crystals for the cooling crystallization process.

$$\dot{Q}_{cc,S_{10}} = \dot{m}_{cc,S_{10}} \cdot Cp_{S_{10}} \cdot (T_{pr} - T_{cc}) \tag{5-76}$$

3. Cooling of the solution for the EFC process of $Na_2SO_4 \cdot 10H_2O$ and ice.

$$\dot{Q}_{EFC,sol} = \dot{m}_{cc} \cdot Cp_{sol} \cdot (T_{cc} - T_{cr}) \tag{5-77}$$

4. Cooling of the formed $Na_2SO_4 \cdot 10H_2O$ crystals for the EFC process.

$$\dot{Q}_{EFC,S_{10}} = \dot{m}_{EFC,S_{10}} \cdot Cp_{S_{10}} \cdot (T_{cc} - T_{cr}) \tag{5-78}$$

5. Cooling of the formed ice for the EFC process.

$$\dot{Q}_{EFC,ice} = \dot{m}_{EFC,ice} \cdot Cp_{ice} \cdot (T_{cc} - T_{cr}) \tag{5-79}$$

6. Formation of the $Na_2SO_4 \cdot 10H_2O$ crystals.

$$\dot{Q}_{cr,S_{10}} = \Delta H_{S_{10}} \cdot \dot{m}_{S_{10}} \tag{5-80}$$

7. Formation of the ice crystals.

$$\dot{Q}_{cr,ice} = \Delta H_{H_2O} \cdot \dot{m}_{ice} \tag{5-81}$$

8. Formation of the sodium nitrate crystals (if applicable).

$$\dot{Q}_{cr,N} = \Delta H_N \cdot \dot{m}_N \tag{5-82}$$

Corrections for more accurate energy calculations for the crystallizer

Rough estimates can be obtained by solving the energy equations above. However, as the amount of formed $Na_2SO_4 \cdot 10H_2O$ gradually increases during the cooling crystallization process and the amount of solution therefore decreases, the concentration of sodium nitrate in solution gradually increases. Similarly, during EFC the amount of solution further decreases and the the sodium nitrate concentration further increases. In this way, more accurate results can be obtained by splitting the cooling crystallization process and the EFC process into n intervals in terms of solution sodium nitrate concentration. All these intervals have the same (small) temperature and concentration difference. The mass fraction of each component i in solution at interval k is then given by:

$$w_{cc,i,k} = w_{pr,i} + (k-1) \cdot \frac{w_{cc,i} - w_{pr,i}}{n} \tag{5-83}$$

And the temperature difference over each interval is given by the difference in the process stream temperature and temperature at the end of the cooling crystallization process, divided by the number of intervals:

$$\Delta T_{cc,k} = \frac{(T_{pr} - T_{cc})}{n} \tag{5-84}$$

The energy for cooling of interval k for the solution, $\dot{Q}_{cc,sol}$, and for the $Na_2SO_4 \cdot 10H_2O$, $\dot{Q}_{cc,S_{10}}$, is then given by.

$$\dot{Q}_{cc,sol,k} = \left(\dot{m}_{pr} - k \cdot \frac{\dot{m}_{cc,S_{10}}}{n} \right) \cdot Cp_{sol,k} \cdot \Delta T_{cc,k} \tag{5-85}$$

$$\dot{Q}_{cc,S_{10},k} = \frac{\dot{m}_{cc,S_{10}}}{n} \cdot k \cdot Cp_{S_{10}} \cdot \Delta T_{cc,k} \tag{5-86}$$

Similarly for the EFC process:

$$w_{EFC,i,k} = w_{cc,i} + (k-1) \cdot \frac{w_{efc,i} - w_{cc,i}}{n} \tag{5-87}$$

In this case the temperature difference over each interval is given by the difference in the temperature at the end of the cooling crystallization process and the operating temperature of the crystallizer, divided by the number of intervals:

$$\Delta T_{EFC,k} = \frac{(T_{cc} - T_{cr})}{n} \tag{5-88}$$

The energy for each interval is then given by:

$$\dot{Q}_{EFC,sol,k} = \left(\dot{m}_{cc} - k \cdot \frac{\dot{m}_{EFC,S_{10}} + m_{EFC,ice}}{n} \right) \cdot Cp_{sol,k} \cdot \Delta T_{EFC,k} \tag{5-89}$$

$$\dot{Q}_{EFC,S_{10},k} = \frac{\dot{m}_{EFC,S_{10}}}{n} \cdot k \cdot Cp_{S_{10}} \cdot \Delta T_{EFC,k} \tag{5-90}$$

$$\dot{Q}_{EFC,ice,k} = \frac{\dot{m}_{EFC,ice}}{n} \cdot k \cdot Cp_{ice} \cdot \Delta T_{EFC,k} \tag{5-91}$$

The total energy consumption for cooling and crystallization, including the 10% heat loss, can be obtained with the following equation:

$$\begin{aligned}\dot{Q}_{\text{cooling}} = 1.1 \cdot \Bigg(& \sum_{k}^{n} \dot{Q}_{cc,sol,k} + \sum_{i}^{n} \dot{Q}_{cc,S_{10},k} + \sum_{k}^{n} \dot{Q}_{EFC,sol,k} \\ & + \sum_{k}^{n} \dot{Q}_{EFC,S_{10},k} + \sum_{k}^{n} \dot{Q}_{EFC,ice,k} + \dot{Q}_{cr,S_{10}} + \dot{Q}_{cr,ice} \Bigg)\end{aligned} \tag{5-92}$$

Heating energy for the calcium precipitation process and sodium nitrate product.

The precipitation process takes place at $\#°C$. However, the bleed stream from the EFC crystallizer has a temperature equal to the operating temperature of the crystallizer. Therefore, the bleed stream needs to be heated:

$$\dot{Q}_{bl} = \dot{m}_{bl} \cdot Cp_{bl} \cdot (20 - T_{cr}) \tag{5-93}$$

The nitrate salt product is a concentrated solution and for selling purposes, the water content is evaporated out of the sodium nitrate product. Therefore, the energy for heating includes the energy for evaporation of the water from the sodium nitrate product.

$$\dot{Q}_{\text{evap}} = \dot{m}_{P,N} \cdot \Delta H_{vap,H_2O} \tag{5-94}$$

The total energy for heating is then given by:

$$\dot{Q}_{\text{heating}} = \dot{Q}_{bl} + \dot{Q}_{\text{evap}} \tag{5-95}$$

5-2 Dimensioning of equipment and fixed costs

The capital cost estimation for chemical process plants can and is often based on estimates of the major equipments. In this case, the process model can be used to determine magnitude of the streams to and from the different process equipments and the required cooling capacity. In turn, this will result in size estimates for the different equipment items. Therefore, this so called 'factorial method of cost estimation' can be applied [48]. The estimates of the capital cost will become more accurate in the next stages of the project, when more detailed specifications and firm quotations are available.

The total capital costs of plant can be expressed as a function of the costs of the major equipment items and corrected with an installation factor:

$$CAPEX = F \cdot \sum C_E \tag{5-96}$$

With C_E the fixed costs for the individual major process equipment items and F the installation factor, which typically as a value of # for a mixed fluids-solids processing plant[48][47].

In the following subsections the formulas for the fixed costs for the different equipment items is presented. For most of the items a cost formula in the form of equipment 5-97 can be determined with quotations of similar equipment items [48][47].

$$C_E = C_B \left(\frac{Q}{Q_B} \right)^n \tag{5-97}$$

With C_B the known base cost for equipment with capacity Q_B. n is a scaling coefficient which depends on the type of equipment.

5-2-1 EFC crystallizer and cooling machine

The EFC crystallizer is a costly piece of equipment consisting scraped cooled surfaces inside a vessel. Estimating the costs for the crystallizer is somewhat difficult as the EFC crystallizer is a custom made piece of equipment of which none have been made in the size required for this project. Therefore the costs for the EFC crystallizer are rough estimates at best. The best option is to base the cost for the crystallizer on the capacity of the crystallizer in terms of feed flow and relate this to the quotation of another industrial EFC crystallizer.

The information of one EFC crystallizer with a capacity of 200L/hr was provided. Using a scaling coefficient of 0.4 as is typical for jacketed reactors, the costs of the EFC crystallizer can be estimated with the following equation:

$$C_{\text{cryst}} = \# \cdot \left(\frac{m_{\text{feed}}}{\#}\right)^{0.4} \tag{5-98}$$

Cooling is supplied by a cooling machine and the costs for a cooling machine depend on the cooling duty and operating temperature. From quotations of cooling machines of different sizes, an equation to determine the costs for a cooling machine was determined. In table 5-1 the cost information of two quotations for cooling machines is provided.

Table 5-1: Quotations for two cooling machines with similar operating temperatures but different capacities.

Investment	Capacity refr.	COP
€#	1240 kW	2.22
€#	127 kW	1.90

$$\# = \# \cdot \left(\frac{1240}{127}\right)^{n} \tag{5-99}$$

With n the exponential scaling factor, solving the above equation gives n = #. The costs for a cooling machine with a capacity of $\dot{Q}_{tot}$ is then given by:

$$C_{\text{cooling mach.}} = \# \cdot \left(\frac{\dot{Q}_{tot}}{127}\right)^{\#} \tag{5-100}$$

5-2-2 Buffer vessel

The volume of the buffer vessel is determined by the dissolution time of sodium hydroxide, which was found to be about # min, and the incoming feed stream. However, as the salt sludge separation process is connected after after the HyVent Metal recovery process, the buffer vessel is also used to compensate for discontinuities in the feed stream from the HyVent process. A rule of thumb is that a half-full residence time of # - # minutes is appropriate for vessels between two processes[49]. Therefore a half-full residence time of # minutes is chosen. The largest of the

$$V_{\text{buffer}} = \frac{\dot{m}_{\text{feed}} \cdot \tau_{NaOH}}{\rho_{\text{feed}}} \tag{5-101}$$

or

$$V_{\text{buffer}} = \left(\frac{\dot{m}_{\text{feed}} \cdot \tau_{\text{half}}}{\rho_{\text{feed}}} \right) \cdot 2 \tag{5-102}$$

The largest volume from the two equations determines the buffer vessel volume. In table 5-2 the quotations of two buffer vessel are provided by EFC Separations BV, which can be used to develop an equation for the cost of the buffer vessel.

Table 5-2: Quotations for two buffer vessel width different volumes.

Investment	Volume
€#	1000 L
€#	500 L

$$\# = \# \cdot \left(\frac{1000}{500} \right)^n \tag{5-103}$$

With n the exponential scaling factor, solving the above equation gives n = #. The costs for a buffer vessel with a volume of V_{buffer} is then given by:

$$C_{\text{buffer}} = \# \cdot \left(\frac{V_{\text{buffer}}}{0.5} \right)^{\#} \tag{5-104}$$

5-2-3 Precipitation vessel

In the precipitation the incoming bleed stream is heated to $\#^{\circ}C$and calcium oxide and nitric acid are dosed to the solution. Therefore, a jacketed agitated reactor can best be used as precipitation vessel.For the precipitation process, a residence time of # minutes was found sufficient. The volume of the precipitation vessel is then given by:

$$V_{\text{precip}} = \tau_{\text{precip}} \cdot \dot{m}_{bl} \cdot \rho_{bl} \tag{5-105}$$

The costs for a stainless steel jacketed and agitated reactor vessel can be determined with the following equation[50]:

$$C_{\text{precip}} = \# \cdot (V_{\text{precip}} \cdot \#)^{\#} \tag{5-106}$$

5-2-4 Design of settling device

After the molybdate and vanadate have precipitated out of the stream, the next step is to separate the remaining stream from these formed solids. As the formed solids are rather small, most filtrate technologies are not applicable, while a settling device is (fig. 5-3).

Gravitational forces cause the particles to accelerate until a combination of the frictional drag in the fluid and buoyancy force balance the gravitational force. Under the assumption that the solid particles can be represented by solid spheres, the terminal settling velocity can be determined with the following equation [47]:

Figure 5-3: Gravity settler for the separation of liquid- solid mixtures [47]

$$\rho_P \frac{\pi d^3 g}{6} = \rho_F \frac{\pi d^3 g}{6} + c_D \frac{\pi d^2}{4} \frac{\rho_F v_T^2}{2} \tag{5-107}$$

Where, ρ_P = particle density (kg/m^3)
ρ_F = fluid density (kg/m^3)
d = particle size (m)
C$_D$ = drag coefficient (-)
v$_T$ = terminal settling velocity (m/s)

This equation can be rearranged to obtain the terminal velocity:

$$v_T = \sqrt{\frac{4gd}{3c_D} \frac{\rho_P - \rho_F}{\rho_F}} \tag{5-108}$$

The drag coefficient is dependent on the Reynolds number:

- **Laminar flow (Re$\leq$ 2):** For rigid spheres in a laminar flow the drag coefficient can be determined according to Stoke's law:

$$c_D = \frac{24}{Re} = \frac{24\mu_F}{d v_T \rho_F} \tag{5-109}$$

- **Turbulent flow (2 $\leq$Re$\geq$ 500):** For Reynolds number above 2 the drag coefficient can be determined with the following empirical expression [47]:

$$c_D = \frac{18.5}{Re^0.6} \tag{5-110}$$

- **Higher level of turbulence (Re$\geq$ 500):** For Reynolds number above 500 the drag coefficient becomes:

$$c_D = 0.44 \tag{5-111}$$

With the determined terminal settling velocity, the length and width (assume L = W) of the settler and the residence time can be determined:

$$L_{\text{settler}} = \left(\frac{m_{bl}}{v_T \cdot \rho_F} \right)^{1/2} \tag{5-112}$$

$$\tau_{\text{settler}} = \frac{H_{\text{settler}}}{v_T} \tag{5-113}$$

Where H is the height of the settler and can be chosen by the user. A minimal height of 1m is required for maintenance.
The volume of the settler is then given by:

$$V_{\text{settler}} = L^2_{\text{settler}} \cdot H_{\text{settler}} \tag{5-114}$$

The volume of the vessel is used to determine the costs fo the vessel. As the stream is corrosive to normal carbon steel, stainless steel 316 is used as material. According to several quotations from EFC Separations B.V. the costs for a stainless steel settler is €# per m^3 with a base price of €#.

$$C_{\text{settler}} = \# \cdot (V_{\text{settler}})^{\#} \tag{5-115}$$

5-2-5 Vacuum belt filters

The costs for a vacuum belt filter can be estimated by the required filtration area. The filtration area in turn depends on the mass flow of the slurry to the filter, the solid fraction of the slurry and an empirical factor that relates the mass flow to the filter area:

$$A_{filt,i} = e_{belt} \cdot \dot{m}_{sl,i} \tag{5-116}$$

With subscript *i* indicating the filter area for either the ice filter or the salt filter.
Prices for filters of different sizes were provided by the company Outotec, varying from #k euro to #k euro. The equation for the costs for the belt filters can be determined with the information from two quotations (table 5-3):

Table 5-3: Quotations of two vacuum belt filters of different sizes.

Investment	Filter area
€#	10.15 m^2
€#	0.1 m^2

$$\# = \# \cdot \left(\frac{10.15}{0.1}\right)^{n} \tag{5-117}$$

Solving the equations above results in an scaling coefficient of n = #. This results in the following equation to determine the costs of a vacuum belt filter with a filter area of $A_{filt,i}$:

$$C_{filt,i} = \# \cdot \left(\frac{A_{filt,i}}{0.1}\right)^{\#} \tag{5-118}$$

5-3 Energy and raw material consumption and variable costs

The energy consumption of the process consists of the energy required for cooling, $\dot{Q}_{cool}$, in the EFC crystallizer, the energy for heating of the bleed stream to # $°C$and evaporating the water out of the sodium nitrate product.
The electrical power for cooling can be determined with the COP of the cooling machine. The COP relates the cooling duty to the electrical power required to deliver this cooling duty. The COP of a cooling machine depends on the condensing temperature and evaporation temperature of the refrigerant and was determined with the program CoolPack.
The average annual operating hours for continuous processes is estimated to be 8000 hr/yr. The yearly total energy consumption in kWh of the process is then given by:

$$\dot{W}_{el,total} = \left(\frac{\dot{Q}_{\text{cooling}}}{COP_{\text{cool}}} + \dot{Q}_{\text{heating}}\right) \cdot 8000 \tag{5-119}$$

The price per kWh is around €# [51].

The raw material flows are converted to tonnes per year, with 8000 operational hours annually. The price per tonne for the different raw materials, i.e. sodium hydroxide, calcium oxide and nitric acid, are averaged prices from bulk chemical vendors [52] [53] [54].

The total variable costs are then given by:

$$VC = C_{\text{energy}} + C_{\text{raw materials}} \tag{5-120}$$

5-4 Product flow and revenue

Four product flows can be identified, of which only two can be sold to the market: The ice/water product is recycled to the HyVent Metal Recovery process and the calcium

precipitate product stream is considered as a waste product since a mixture of calcium molybdate, calcium vanadate and calcium sulfate is formed, beside the fact that this product stream is very small when compared to the other product streams.
The sodium sulfate decahydrate product can directly be sold to the market, while the sodium nitrate stream first has to be turned into a solid product by evaporation. This reduces the sodium nitrate product with about #%.
The product streams are converted to tonnes per year and the prices are again estimated from bulk chemical vendors [55] [56]. However, the prices are heavily dependent on the purity of the products. The sodium sulfate decahydrate product is relatively constant. The purity of the sodium nitrate product, however, depends strongly on the operating temperature of the EFC crystallizer: A high operting temperature (e.g. -10°C) results in a high contamination of sodium sulfate (about #w%) in the sodium nitrate product, while an operating temperature close to the ternary eutectic point has only a low concentration of sodium sulfate (about #w%). Therefore, a range of prices was found for a ranging sodium nitrate purity. This data was plotted and a fitting curve was applied to this data:

$$\begin{aligned} C_{NaNO_3} = \# \cdot 10^-5 \cdot \left(\frac{w_{PN} - 99.8}{-0.1}\right)^{\#} - \# \cdot \left(\frac{w_{PN} - 99.8}{-0.1}\right)^{\#} \\ - \# \cdot \left(\frac{w_{PN} - 99.8}{-0.1}\right)^{\#} - \# \cdot \left(\frac{w_{PN} - 99.8}{-0.1}\right) + \# \end{aligned} \tag{5-121}$$

Below a purity of#% the price of sodium nitrate is maintained at €#/tonne.

For the sodium sulfate product, the following equation was derived for the market value:

$$C_{Na_2SO_4 \cdot 10H_2O} = \# \cdot \left(\frac{w_{PS} - 99.6}{-0.1}\right)^{\#} + \# \cdot \left(\frac{w_{PS} - 99.6}{-0.1}\right)^{\#} - \# \cdot \left(\frac{w_{PS} - 99.6}{-0.1}\right) + \# \tag{5-122}$$

Below a purity of #% the price of the sodium sulfate product is maintained at €#/tonne.

5-5 OPEX and Pay Back time of the process

the operating expenditures, or OPEX, of the process are variable costs together with the labour costs (€# per FTE), maintenance (#% of CAPEX) and depreciation of the equipment (#% of CAPEX, depreciation time of 10 years):

$$\text{OPEX} = VC + \# \times \text{CAPEX} + \# \tag{5-123}$$

The Net Profit is the revenue that remains after the deduction of the operating expenses and is used to determine the Pay Back time of the process and the Net margin. The Net margin is the percentage of revenue that is turned into profit.

$$\text{Pay Back} = \frac{\text{CAPEX}}{\text{Net Profit}} \tag{5-124}$$

$$\text{Net margin} = \frac{\text{Net Profit}}{\text{Revenue}} \tag{5-125}$$

Chapter 6

Model results and optimization of the process

For confidentiality purposes, most results have been left out of this report

The model equations from the previous chapter can be used to determine the flow rate, temperature and composition of all the streams in the process. Subsequently the cooling duty, raw material consumption and product flows and purities can be determined and the economic potential of the process can be studied for different operating conditions.

In order to evaluate different process design options in terms of yield, variable costs and fixed costs, the developed process model can be used, reconfigured and optimized. In this chapter and the next, this model will be used as a tool to answer the following sub-questions:

- What process options for a continuous process can be identified to separate the aqueous solution, representing the HyVent metal recovery process stream?
- What are the optimal operating conditions for the process.
- What recovery of the different salts can be obtained and what options are there for sequential removal of salts from the solution in a continuous EFC process.
- Evaluate the different process options for energy consumption, cost of equipment, raw material use.

6-1 Model results

In figures 6-1 to 6-3 the product purity and product flow of the concentration sodium nitrate solution, sodium sulfate decahydrate salt product and ice product, respectively, are plotted against a range of operating temperatures.

The sodium nitrate product purity increases as the operating temperature of the crystallizer decreases, while the mass flow reduces. This can be explained by the changing composition of the mother liquor in the crystallizer: A lower temperature corresponds to a composition closer to that of the ternary eutectic point, where the sodium nitrate concentration has a maximum, while sodium sulfate has a minimum value at that point. Therefore, as the operating temperature decreases, so does the sodium sulfate concentration in the bleed stream leaving the crystallizer, resulting in a higher purity for the sodium nitrate concentrated solution.

The mass flow of the nitrate product decreases as at a lower operating temperature more sodium sulfate decahydrate and ice have left the solution, leaving a smaller bleed stream from the crystallizer.

The sodium sulfate decahydrate product purity and ice product purity decrease with a decreasing operating temperature. This can be explained by the composition of the mother liquor that is entrapped in the crystal product, which becomes higher in sodium nitrate and reduces in sodium sulfate and water composition.

The ice product mass flow increases for a decreasing operating temperature as during an EFC process, the amount of ice and salt that is formed corresponds the composition of the mother liquor. In this case, the sodium sulfate concentration decreases proportional to the operating temperature and therefore the fraction of ice that forms increases.

At a temperature of $\# \ ^\circ C$ the sodium nitrate product flow shows a steep decrease and similar changes can be observed in the sodium sulfate graph. These changes are the result of operating at (or just below) the ternary eutectic point of sodium nitrate, sodium sulfate and water: The sodium sulfate decahydrate product becomes contaminated with sodium nitrate salt, causing a steep drop in the sodium sulfate decahydrate product purity, while at the same time the total amount of formed salts increase, resulting in a larger mass flow for the sodium sulfate decahydrate product and a lower mass flow for the sodium nitrate concentrated solution.

nitr_prod.jpg

Figure 6-1: Sodium nitrate concentrated product stream purity and mass flow for a varying crystallizer operating temperature.

sulf_prod.jpg

Figure 6-2: Sodium sulfate decahydrate product purity and mass flow for a varying crystallizer operating temperature.

ice_prod.jpg

Figure 6-3: Ice product purity and mass flow for a varying crystallizer operating temperature.

In figures 6-4 the effect of a varying feed flow is shown on the concentrated sodium nitrate stream product. As can be observed, the response of the product flow is directly proportional to the feed flow, while the purity remains unaffected. Similar results were found for the ice product and sodium sulfate decahydrate product flow and purity.

`nitr_feed.jpg`

Figure 6-4: Sodium nitrate concentrated product stream purity and mass flow for a varying feed flow.

6-2 Options for optimization

The EFC crystallizer operating temperature can be varied and increasing this temperature on one hand reduces the energy for cooling, but on the other hand decreases the sodium sulfate decahydrate production. Also, the remaining mother liquor has a higher sodium sulfate concentration for a higher operating temperature. In terms of costs, the This can be translated to:

1. Reduced energy costs
2. Reduced income from sodium sulfate decahydrate product as the production is lower.
3. Reduced income from sodium nitrate concentrated product stream as this stream is contaminated with more sodium sulfate, reducing the sell price.

An objective equation can be formulated to find the optimal operating temperature of the EFC crystallizer. In this case, the objective function is to maximize the economic potential of the process, therefore, the objective function is to maximize the Net Profit for a range of operating temperatures of the EFC crystallizer:

$$\text{Net Profit} = \text{Revenue} - \text{OPEX} \tag{6-1}$$

The OPEX and Revenue are, of course, dependent on many different variables of the process. Therefore the process model is used to determine at which operating temperature the Net Profit is largest. Results are calculated for operating temperatures varying from -10 to -17.6$°C$with step size of 0.1$°C$. The results for each operating temperature were stored and the maximum value was determined together with the corresponding temperature. In figure 6-5 the Net Profit vs. the operating temperature is plotted.

Figure 6-5 clearly shows that the optimal operating temperature as very near the temperature of the ternary eutectic point of sodium nitrate, sodium sulfate decahydrate and water. Operating below the ternary eutectic point, however, decreases the net profit of the process. This can be explained by market price of the sodium nitrate product and the purity of this product, as the purity increases for a lower operating temperature. Also, the sodium sulfate decahydrate product is larger at a lower operating temperature. At the ternary eutectic point, however, the sodium sulfate product is contaminated with sodium nitrate, reducing its value as well as reducing the sodium nitrate product stream, resulting in reduced profits. Therefore, as the model has determined, the optimal operating temperature of the crystallizer is at $\#°C$, $\#°C$above the ternary eutectic point to ensure no sodium nitrate crystallization takes place.
In table 6-1 the results for costs and revenue for the optimized process are shown. These are discussed at the end of this chapter, after heat integration has been applied.

Net_profit.jpg

Figure 6-5: Net profit for a varying crystallizer operating temperature.

6-3 Possibilities for heat integration

Heat integration can reduce the energy consumption of a process by heat transfer from a hot input stream to a cold product stream. In this process several hot and cold streams can be identified:

- Hot: Feed stream to the process
- Hot: Process stream to the EFC crystallizer

Table 6-1: Costs and Revenue for the process with optimized operating temperature for a feed flow of #m^3/hr.

Description	Cost/Revenue
CAPEX	
OPEX:	
energy	
raw materials	
REVENUE	
Sodium nitrate	
Sodium sulfate decahydr.	
Net Profit	
Net margin	
Pay back time	

- Cold: Ice product stream
- Cold: Sodium sulfate decahydrate stream
- Cold: Bleed stream from the EFC crystallizer.

Not of all of these streams are suitable for heat integration. For example the feed stream: As the sodium nitrate concentration in this stream is relatively low and the sodium sulfate concentration is relatively large, one should take care not to cool this stream to much as cooling crystallization of sodium sulfate might occur inside the heat exchanger. A safer option for heat integration would be for the hot process stream to the EFC crystallizer. In this stream the sodium nitrate concentration is much higher than for the feed stream and the sodium sulfate concentration lower, resulting in a much lower crystallization temperature for cooling crystallization.
Two of the three cold streams are solid products and although the heat capacity of solids or a slurry is higher than for most solution, heat transfer with solids or a slurry is much lower [57][58]. The bleed stream does not contain solid particles and this stream needs to be heated to $\#°C$for the precipitation process. Therefore, heat integration can best be applied between the hot process stream and the cold bleed stream.

It is assumed that cooling crystallization commences at a temperature of $\#°C$. The bleed stream should therefore be heated to a maximum temperature of $\#°C$. The total amount of heat transferred to the bleed stream. $\dot{Q}_{int}$ is then given by:

$$\dot{Q}_{int} = \dot{m}_{bl} \cdot Cp_{bl} \cdot (\# - T_{bl}) \tag{6-2}$$

The overall heat transfer coefficients for water and brine is around 600 W/(m^{2}K) [48] and the logarithmic mean temperature difference between the two streams is given by:

$$\Delta T_{lm} = \frac{(T_{pr,1} - T_{bl,2}) - (T_{pr,2} - T_{bl,1})}{ln\frac{(T_{pr,1} - T_{bl,2})}{(T_{pr,2} - T_{bl,1})}} \tag{6-3}$$

The required heat transfer area of the heat exchanger is then:

$$A_{\text{HEX}} = \frac{\dot{Q}_{int}}{({}^{U}/_{1000} \cdot \Delta T_{lm})} \tag{6-4}$$

The heat transfer area of the heat exchanger can be used to estimate the costs of the heat exchanger, depending on the type of exchanger. In this case a simple shell and tube fixed U-tube heat exchanger is used. The material is stainless steel 316 as the streams are corrosive to standard carbon steel. An overview of the results are shown in table 6-2.

Table 6-2: Numerical results for the heat integration between the bleed stream and the process stream.

	T_in [°C]	T_out [°C]	$\dot{m}$ [kg/s]
Bleed stream			
Process stream			
$\dot{Q}_{int}$ [kW]			
ΔT_{lm}			
U [W/(m^{2}K)]			
A$_{HT}$ [m^2]			
CAPEX HEX		€	
OPEX HEX		€	
Energy saved [kWh/yr]			
Energy cost saving		€	
Total annual saving		**€**	
Pay Back time HEX			

The energy savings are twice that of the heat exchanged. The pay back time of the heat exchanger was calculated as function of the energy savings resulting from the heat integration. The results show that for a small investment an annual savings can be ensured equal to almost #% of the total net profit of the the process. The pay back of the heat exchanger is only # year, making this a economically justified option for heat integration.

6-3-1 Comparison of results

The process design with heat integration is shown in figure 6-6. The process is operated at the optimized operating temperature of #°C. The economical evaluation of the process is shown in table 6-3.

Both processes, i.e. with or without heat integration, show a positive Net Profit. The pay back time, however, is # years and rather high. Ideally this should be under # years. Applying the earlier discussed heat integration, increases the profitability of the process and decreases its pay back time.
In the next chapter, this design is compared to two alternative process configurations where multiple crystallizers are used.

PFD-EFC-finaldesign.jpg

Figure 6-6: Flow diagram of the process design for the salt sludge separation, including heat integration.

Table 6-3: Numerical results for the process design with and without heat integration for a feed flow of #m^3/hr..

	No Heat integration	Including heat integration
CAPEX		
OPEX:		
energy		
raw materials		
REVENUE		
Sodium nitrate		
Sodium sulfate decahydr.		
Net Profit		
Net margin		
Pay back time		

Chapter 7

Case studies and Final process design

For confidentiality purposes, most results have been left out of this report

In the previous chapter the process with one crystallizer was presented and for reference purposes is from now referred to as case study 1. In this process ice and sodium sulfate decahydrate were produced as solid products and sodium nitrate as a concentrated solution. The economical evaluation of this process has shown that the sodium nitrate product generates most of the revenue. However, before it could be sold as a solid product, first the water content had to be evaporated from the concentrated solution. A more profitable process could be obtained by producing sodium nitrate crystals in an EFC process instead of leaving it in the concentrated solution. Also, the entire crystallization process is conducted in one large EFC crystallizer, while the cooling crystallization process also could be done in a cheaper cooling crystallization vessel. This would reduce the size of the EFC crystallizer and could improve the product of tresult in a more profitable process. In order to study if the proposed changes result in a more profitable process, two case studies are proposed and elaborated.

7-1 Case study 2: Cooling crystallization and EFC in separate crystallizers

As most of the sodium sulfate decahydrate is formed in the cooling crystallization process, the process in this case study contains two crystallizer: A cooling crystallizer and an EFC crystallizer, in figure 7-1 a flow diagram of the process is shown. In this configuration, cooling crystallization is done in a vessel at relatively high temperature and in a low cost crystallizer when compared to the same process in an EFC crystallizer. The remaining solution after the cooling crystallization process is fed to an EFC crystallizer which operates at the optimal temperature determined in case study 1 and thus produces the remaining sodium sulfate decahydrate (and the ice). The advantage of the two different crystallizers is that the majority of the sodium sulfate decahydrate salt is formed in a separate vessel, which could result in a higher purity of the salt.

`PFD-EFC_CCandEFC.jpg`

Figure 7-1: Flow diagram of the process as described in the second case study: A cooling crystallizer is configured in series with an EFC crystallizer.

In table 7-2 the results of the process are presented together with those of the other two cases and will be discussed after the third case study has been introduced.

7-2 Case study 3: Two EFC crystallizers connected in series

The process design from the previous chapter has shown that operating at the ternary eutectic point of sodium nitrate, sodium sulfate decahydrate and water resulted in loss of profit as on one hand the produced mixed sodium sulfate decahydrate and sodium nitrate salts had a low market value and on the other hand the concentrated sodium nitrate product was lower than for an operating temperature above the ternary eutectic point.

In this case study two EFC crystallizers are connected in series (fig. 7-2). The first crystallizer operates at the same temperature as that of the original process, i.e. $\# \, ^{\circ}C$, and therefore the sodium sulfate concentration of the mother liquor is reduced to a minimum, i.e. that of the ternary eutectic point. The second crystallizer operates slightly below the ternary eutectic point, producing sodium nitrate and very little amounts of sodium sulfate decahydrate in the ratio of the composition of the mother liquor at that point. In this way, the sodium nitrate salt could have a higher purity than the sodium nitrate product from the concentrated solution. A disadvantage is of course the high cost of a second EFC crystallizer. This case study will show if the cost of a second EFC crystallizer can be overcome by the production of a more pure sodium nitrate salt product.

`PFD-EFC_EFCandEFC.jpg`

Figure 7-2: Flow diagram of the process as described in the third case study: Two EFC crystallizers connected in series.

7-3 Case study results and Final process design

In table 7-1 and table 7-2 the results of this case study are shown together with those of the previous cases. In appendix B a more detailed overview of the different cost components are provided for the three cases.

In table 7-1 the annual sodium nitrate and sodium sulfate decahydrate product flows are shown together with the purity of the product and corresponding market value. For the process of the first case study, all the sodium nitrate comes from the evaporating concentrated sodium nitrate stream, just as is the case for the second case study. For the third case, where sodium nitrate is also formed in the EFC crystallizer, the sodium nitrate flow from the concentrated bleed stream is much smaller. The purity is somewhat higher than for the original process (# higher), this can be explained as in case study 3 the mother liquor has the composition of that of the ternary eutectic point, which is the minimal sodium sulfate concentration in the mother liquor. The processes of case studies 1 and 2 operate slightly above this point and therefore have a somewhat higher sodium sulfate concentration and thus lower purity.

In case study 2, the sodium sulfate decahydrate formed in the cooling crystallizer has, as expected, a higher purity. This can be explained by the mother liquor composition in the cooling crystallizer vessel, which has a much lower sodium nitrate concentration than in the EFC crystallizer. therefore, the mother liquor still present in the salt product reduced the purity less than the for the sodium sulfate decahydrate formed in the EFC crystallizer.

In case study 3, crystallization of sodium sulfate is continued until close to the ternary eutectic point, similar to case 1. The sodium nitrate formed in the second EFC crystallizer is only contaminated by low amounts of sodium sulfate decahydrate. However, the mother liquor still present in the sodium nitrate salt reduced the purity to a value below that of the sodium nitrate product resulting from the concentrated solution.

Unfortunately, the recovery of water is not #% for all three cases, meaning that a zero liquid discharge process was not achieved. However, for case 3 a recovery of above #% was reached. For case 1 and 2 this was only #%. The difference can be explained by the EFC process that, for case 3 was continued longer than was the case at the process of cases 1 and 2.

The Recovery of sodium nitrate is almost equal for cases 1 and 3, while for case 2 the recovery of sodium nitrate was very low: As the nitrate salt at case 2 has such a low purity, it was decided not to count it as 'recovered valuable compound' but more as waste product with some market value and therefore only the sodium nitrate form the concentrated sodium nitrate product was taken into account for the recovery.

The recovery of the both sodium nitrate and sodium sulfate is somewhat higher for case study 3, which can also be explained by the EFC process that continues to a lower temperature than for the other cases.

In table 7-2 the financial results of the three case studies can be found. The capital expenses increase for case 1 to case 3: The process of case study 1 has the lowest CAPEX which can of course be explained by the use of only one crystallizer. For case study 2 the CAPEX increases due to the costs for a cooling crystallizer vessel, cooling machine and additional belt filter. For case 3 two EFC crystallizers are used and this results in an even higher CAPEX than for case study 2 as an EFC crystallizer is more expensive than a cooling crystallizer as well as a the additional cooling machine.

The OPEX for case 3 is lower than for case study 2 and this can be explained by the costs for energy and raw materials: As the bleed stream from the (second) EFC crystallizer is smaller for case 3 than for case 2, the heat that is required to ensure a bleed stream temperature of $20°C$for the precipitation process is also lower. Besides the heating for the bleed, another factor reduces the energy costs for case 3, namely the amount of energy required for evaporating the water out of the sodium nitrate concentrated product stream is also lower due to the smaller flow. The raw material costs for calcium oxide and nitric acid are reduced for the same reason. The OPEX of case 1 is smaller than for

Table 7-1: Annual product flow, purity and value per tonne of product for the three cases. The recovery for each component is given as amount of pure product vs. the amount of feed of that component

Case study 1: one EFC crystallizer			
	Flow [t/yr]	Purity [%]	Product value [€/t]
Sodium nitrate			
Sodium sulfate decahydr.			
Recovery H2O			
Recovery NaNO3			
Recovery Na2SO4			
Case study 2: cooling crystallizer followed by EFC			
	Flow [t/yr]	Purity [%]	Product value[€/t]
Sodium nitrate			
Sodium sulfate decahydr. EFC			
Sodium sulfate decahydr. CC			
Recovery H2O			
Recovery NaNO3			
Recovery Na2SO4			
Case study 3: EFC of Na_2SO_4 followed by EFC of $NaNO_3$			
	Flow [t/yr]	Purity [%]	Product value [€/t]
Sodium nitrate			
Sodium sulfate decahydr.			
Sodium nitrate from EFC			
Recovery H2O			
Recovery NaNO3			
Recovery Na2SO4			

case study 3 as the CAPEX costs are simply much lower.
The revenue is largest for case study 2, as the purity of the majority of the sodium sulfate decahydrate was higher than for the other cases.
The CAPEX, OPEX and Revenue result in a Net Profit for case study 1 that is about €# above the Net Profit of case study 3. As both the CAPEX and Net Profit are more favourable for the process of case study 1, the pay back time is also lower for case study 1, which is still high (# years). In figure 7-3 the prospected total profit is shown for 35 operational years and the result clearly shows that the process of case study 1 is the economically most profitable process design option for the salt sludge separation process.

Table 7-2: Numerical results for case study 3, shown next to the results of the previous case study and original process

	Case study 1: One EFC crystallizer	Case study 2: CC and EFC	Case study 3: EFC and EFC
CAPEX			
OPEX			
energy			
raw materials			
REVENUE			
Sodium nitrate			
Sodium sulfate decahydr.			
Net Profit			
Net margin			
Pay back time			

7-4 Case 4: Discharge the brine, no process and no treatment

Ultimately, it is interesting to study the benefits of the previous cases when compared to a case for which the brine from the HyVent metal recovery process is not treated at all. This would involve the costs for processing of the brine by a third party or an environmental fine of some sort per cubic meter discharged brine. In this way the net savings of the salt sludge separation process can be determined and an evaluation can be made to decide whether or not to continue with this project.

The prices for the discharge of brine differ greatly between location, brine content and concentrations. A mean price of €#/tonne is assumed as this price was encountered in different projects of EFC Separations, although in reality the price might by a lot higher due to the vanadium content in the brine. For a feed of #m^3/hr this would result in an annual loss of:

$$C_{\text{discharge}} = 2 \cdot 8000 \cdot \text{€}\# = \text{€}\ \# \tag{7-1}$$

These costs can also be plotted in the graph of figure 7-3 and it can be observed that after 2 operating years, the savings resulting from the process of case study 1 are already higher than the costs would be for discharging the brine.

profit_comp.jpg

Figure 7-3: Prospect of generated profits of the processes of case studies 1 to 3 for 35 operating years. The purple lines shows the loss for the case when the brine is untreated and discharged.

Chapter 8

Conclusions and Recommendations

For confidentiality purposes, most results have been left out of this report

8-1 Conclusions

The crystallization behaviour of the system of sodium nitrate, sodium sulfate and water, and the system of potassium nitrate, potassium sulfate and water, were studied in the presence of sodium molybdate and sodium vanadate traces (# - # ppm). Their eutectic points were found and validated with literature. The eutectic points of the pure systems corresponded well to the data from literature, while the addition of sodium molybdate and sodium vanadate caused the composition and temperature of the ternary eutectic points of sodium nitrate, sodium sulfate decahydrate and water, and potassium nitrate, potassium sulfate and water, to change. An explanation for this could be the common ion effect, but this theory needs verification as no literature was available to confirm this behaviour and very little information was available for these systems with sodium molybdate and/or sodium vanadate.
In the sodium sulfate decahydrate crystals, build up of sodium molybdate and sodium vanadate was observed. Washing of the crystals with water reduced the sodium vanadate build up, however, a significant amount of sodium molybdate was still present in the crystal lattice of sodium sulfate decahydrate. In the potassium sulfate crystals, the uptake of molybdate and vanadate was lower.

In the sodium system, the molybdate and vanadate concentration were successfully reduced by the addition of calcium oxide to the solution. Calcium molybdate and calcium vanadate (and about # % of the solids as calcium sulfate) precipitated and this reduced the concentrations of sodium molybdate and sodium vanadate in the solution to below

# ppm and # ppm respectively. Best results were obtained at a solution pH of #, which was achieved by the addition of nitric acid. A sufficient residence time was found to be # to # min after which the mean particle size of the calcium molybdate, calcium vanadate and calcium sulfate was about # μm.
The molybdate and vanadate in the potassium system were unaffected by the calcium precipitation and the concentration of these components could not be reduced.

Potassium hydroxide was rejected as possible base as the molybdate and vanadate concentrations could not be reduced by calcium precipitation. Also, the potassium hydroxide showed excessive scaling during the EFC batch experiments and showed slow kinetics when compared to the sodium system. Therefore, sodium hydroxide was the base of choice for this process.
A steady state process flow model was developed and optimized to maximize the economic potential of the process. This was achieved by maximizing the Net Profit of the process by varying he operating temperature of the EFC crystallizer. The optimal results were found at an operating temperature of # $°C$, slightly above the temperature of the ternary eutectic point of sodium nitrate, sodium sulfate and water. Operating below this optimal temperature reduced the profitability of the process, as a mixed salt product of sodium nitrate and sodium sulfate decahydrate was produced with low market value.

Heat integration was applied to the process, to pre-cool the hot process stream to the EFC crystallizer with the cold bleed stream from the EFC crystallizer. This resulted in a reduction of energy costs and an increase of the Net Profit of #%. The described heat integration is therefore an improvement to the process which can be economically justified.

Besides the process with only one crystallizer, two more processes were introduced and elaborated, both with two crystallizers of which one of the processes used a cooling crystallizer followed by an EFC crystallizer, while the other process used two EFC crystallizers in series. The results of the three processes were compared and a final, economically best, process design was chosen. Although the processes of case studies 1 and 3 generated almost equal revenues, the higher CAPEX of the process of case study 3 resulted in the process of case study 1 to be the process with the largest economic potential for the salt sludge separation process.
The final process generated an annual Net Profit of €# and had a pay back time of # years. Although the pay back time is long, when compared to the costs for simply discharging the brine, the designed process results in higher savings from year #.
The recovery of water, however, was only #% and therefore not enough to fulfill the objective of a zero liquid discharge process.

To conclude, the process described in this thesis is capable of separation aqueous solutions of sodium nitrate and sodium sulfate into profitable products. However, a zero liquid discharge process was not achieved. The design of a similar process for potassium nitrate, potassium sulfate and water was not achieved.

8-2 Recommendations

The conceptual process design of the salt sludge separation has shown promising results. However, as even my time is limited and no study is ever complete, the following recommendations are proposed for further improvement and validation of the process.

- Experimental determination of heat capacities of sodium sulfate and sodium nitrate at low, sub-zero, temperatures for a range of concentrations. These heat capacities could be an addition to the accuracy of the model, as currently data at a temperature of $25°C$ is used.
- The sodium sulfate salt purity could be improved by washing of the crystals with feed solution or saturated sulfate solution of sodium sulfate. A mother liquor content of about # to #% was observed in the crystal products. By washing the crystals with feed solution, the mother liquor is replaced by a less concentrated solution, effectively reducing the impurity content.
- A more detailed study is required in order to find an explanation of what caused the decrease of the ternary eutectic point in terms of sodium nitrate concentration. In this thesis this decrease was contributed to the common ion effect, but this is only a theory and requires validation.

Bibliography

[1] M. M. Ramirez-Corredores, A. P. Borole, Biocatalysis in Oil Refining, Ch. 2 Conventional refining processes. Studies in Surface Science and Catalysis, volume 164, 2007

[2] U.S. Energy Information Administration. Definitions, Sources and Explanatory Notes - API Gravity. Retrieved from `http://www.eia.gov/dnav/pet/TblDefs/pet_pri_wco_tbldef2.asp`

[3] J. G. Speight, Heavy and Extra-heavy Oil Upgrading Technologies, Ch. 4 Hydrotreating and Desulfurization, 2013, GPP Elsevier

[4] U.S. Energy Information Administration. Percentages of Total Imported Crude Oil by API Gravity. Retrieved from `http://www.eia.gov/dnav/pet/pet_move_ipct_k_a.htm` on 03-10-2016

[5] EPA Emission Standards Reference Guide for on-road and non-road vehicles and engines. Retrieved from `https://www.epa.gov/emission-standards-reference-guide` on 03-10-2016

[6] M. Marafi, a. Stanislaus, "Spent Catalyst waste management: a review Part I - Developments in hydroprocessing catalyst waste reduction and use", Resources, Conservation and Recycling 52, 859-873, 2008

[7] M. Marafi, a. Stanislaus, "Spent Catalyst waste management: a review Part II - Advances in metal recovery and safe disposal methods", Resources, Conservation and Recycling 53, 1-26, 2008

[8] A. Akcil, F. Veglio, "A review of metal recovery from spent petroleum catalysts and ash", Waste management 45, 420-433, 2015

[9] S. Ramirez, P. Schacht, "Leaching of heavy metals under ambient resembling conditions from hydrotreating catalysts", Fuel 110, 286-292, 2013

[10] Buckley, C, "Research into the treatment of inorganic brines and concentrates"'. Water Research Commission Project No. 201, Revision 1021, May 2005.

[11] Lewis, A, Nathoo, J, Reddy, T, Randall, D, Zibi, L & Jivanji, R "Novel technology for recovery of water and solid salts from hypersaline brines: Eutectic freeze crystallization". Water Research Commission Project No. 1727/1/10, August 2010.

[12] A. M. Schwartz, A. S. Myerson,*Handbook of Industrial Crystallization*, *1-Solutions and solution properties*, 2nd edition, Elsevier Science & Technology Books, 2001

[13] H.J.M. Kramer, G.M. van Rosmalen, J.H. ter Horst, *Basic Process Design for Crystallization Processes*, Process & Energy - Separation Technology, TU Delft

[14] J.W. Mullin, *Crystallization*, fourth edition, 2001

[15] E. Wiberg, N. Wiberg, A.F. Holleman, "Inorganic Chemistry", De Gruyter, 1st English ed., 2001

[16] G.L. Stepakoff, D. Siegelman, R. Johnson, W. Gibson, *Desalination* 14 (1974) 25.

[17] A.J. Barduhn, A. Manudhane, *Desalination* 28 (1979) 233.

[18] D.A. Swenne, *The eutectic crystallization of* $NaCl \cdot 2H_2O$ *and ice*, Dissertation, Eindhoven, 1983

[19] van der Ham, F., Witkamp, G.J., de Graauw, J. and van Rosmalen, G.M., *Eutectic freeze crystallization: application to process streams and waste water purification*, Chemical Engineering and Processing, 37(March (2)): 207–213. 1998,

[20] F. van der Ham, G.J. Witkamp, J. de Graauw, G.M. van Rosmalen *Eutectic freeze crystallization simultaneous formation and separation of two solid phases*, J. Cryst. Growth 198–199 (Part 1) (1999) 744–748.

[21] F. van der Ham, M.M. Seckler, G.J. Witkamp, *Eutectic freeze cyrstallization in a new apparatus: the cooled disk column crystallizer*

[22] Vaessen, R.J.C., *Development of scraped eutectic freeze crystallisers*, PhD Dissertation, Delft University of Technology, The Netherlands, 2003a.

[23] J. van Spronsen, M. Rodriguez Pascual, F.E. Genceli, D.O. Trambitas, H. Evers, G.J. Witkamp, *Eutectic freeze crystallization from the ternary Na2CO3–NaHCO3–H2O system. A novel scraped wall crystallizer for the recovery of soda from an industrial aqueous stream.* chemical engineering research and design 8 8 (2 0 1 0) 1259–1263

[24] M. Rodriguez Pascual, F.E. Genceli, D.O. Trambitas, H. Evers, J. Van Spronsen, G.J. Witkamp, *A novel scraped cooled wall crystallizer; Recovery of sodium carbonate and ice from an industrial aqueous solution by eutectic freeze crystallization*, chemical engineering research and design 88 (2010) 1365–1371

[25] M. Rodriguez Pascual, D.O. Trambitas, E. Saez Calvo, H.J.M. Kramer, G.J. Witkamp, *Determination of the eutectic solubility lines of the ternary systm NaHCO3-Na2CO3-H2O*, chemical engineering research and design 88 (2010) 1365–1371

[26] M. Rodriguez Pascual, *Physical Aspects of Scraped Heat Exchanger Crystallizers.* Dissertation, Delft University of Technology, The Netherlands, 2008.

[27] Vaessen, R.J.C., *Development of scraped eutectic crystallizers*, PhD Thesis (TU Delft, Netherlands), 2003b.

[28] C. Himawan, R.J.C. Vaessen, H.J.M. Kramer, M.M. Seckler, G.J. Witkamp, *Dynamic modeling and simulation of Eutectic Freeze Crystallization*, J. Cryst. Growth 237–239 (2003) 2257–2263.

[29] C. Himawan, *Characterization and population balance modeling of Eutectic Freeze Crystallization*, PhD Thesis. Technical University of Delft, The Netherlands, 2005.

[30] Genceli F.E.; Gärtner R.S.; Trambitas D.; Rodriguez M.; Witkamp G.J., *A sustainable technology: Eutectic freeze crystallization - From batch laboratory to continuous industry applications*, Sustainable (Bio)Chemical Process Technology - Incorporating the 6th International Conference on Process Intensification. pp. 235-242, 27-29 September 2005, Delft, The Netherlands.

[31] Genceli F.E.; Rodriguez Pascual M.; Kjelstrup S.; Witkamp G.J., *Coupled heat and mass transfer during crystallization of* $MgSO_4 \Delta 7 H_2O$ *on a cooled surface*, submitted for publication to Crystal Growth & Design.

[32] Genceli F.E.; Hartmann D.; Witkamp G.J.; Berkhout G., *Cyclic Innovation Model Application: Eutectic Freeze Crystallization*, prepared for publication in Separation and Purification Journal.

[33] A.E.Lewis, S.T. Reddy, Recovery of glaubers salt from a reverse osmosis retentate by eutectic freeze crystallization technology, Chemical engineering research and design, 88, 2010

[34] A.E. Lewis, J. Nathoo, K. Thomsen, H.J. Kramer, G.J. Witkamp, S.T. Reddy, D.G. Randall, *Design of a Eutectic Freeze Crystallization process for multicomponent waste water stream*, chemical engineering research and design 88 (2010) 1290–1296

[35] D.G. Randall, J. Nathoo, A.E. Lewis, *A case study for treating a reverse osmosis brine using eutectic freeze crystallization - Approaching a zero waste process* Desalination 266, 2011

[36] Genceli F.E., *Scaling-Up, Eutectic Freeze Crystallization*, PhD thesis. Technical University of Delft, the Netherlands, 2008

[37] J. Nathoo, R. Jivanji, A.E. Lewis, *Freezing Your Brines Off: Eutectic Freeze Crystallization for Brine Treatment*, International Mine Water Conference, Pretoria, South Africa, 2009, pp. 431–437.

[38] W.F. Linke, A. Seidell, Solubilities of Inorganic and Metal Organic Compounds, a Compilation of Solubility Data from Periodical Literature, Van Nostrand Publ., New York, 1965

[39] F.F. Purdon, Aqueous solution and the phase diagram, Butler and Tenner Ltd., London, 1946

[40] K. Thomsen, Electrolyte Solutions: Thermodynamics, Crystallization, Separation methods, Technical University of Denmark, 2008

[41] A.I. Busev, Analytical Chemistry of Molybdenum, Isreal program for scientific translations, Ltd, 1964

[42] G.J. Witkamp, "Crystallization of calcium sulfate and uptake of impurities", Delft university of Technology, 1989

[43] E.Pokorny,"Process of producing calcium molybdate", US 1 873 475, Aug. 23 1932

[44] E.D. Porro,"Process of treating vanadium and molybdenum ores", US 2 823 113, Feb. 11, 1958

[45] G.E.W.K. Steenken, "Process for extracting metals from spent desulphurization catalysts", US 4 087 510, May 2, 1978

[46] M.J. Fernández-Torres, F. Ruiz-Beviá, "Teaching a new technolgy, eutectic freeze crystallization, by means of a solved problem", Education for Chemical Engineers, 7, 2012

[47] R. Smith, "Chemical process, design and integration"', Wiley, 2005

[48] R.K. Sinnott, "Chemical Engineering Design", Coulson & Richardson's Chemical Engineering, Volume 6, 4th edition, 2006

[49] A. Faanes, S. Skogestad, "Buffer tank design for acceptable control performance", Department of chemical engineering, Norwegion university of science and technology, 2003

[50] Matches.com, reactor cost estimate,http://www.matche.com/equipcost/Reactor.html, accessed on 20-11-2016

[51] OVO energy, Average electricity prices around the world,https://www.ovoenergy.com/guides/energy-guides/average-electricity-prices-kwh.html, accessed on 7-11-2016

[52] Alibaba.com, sodium hydroxide, https://www.alibaba.com/showroom/sodium-hydroxide.html, accessed on 7-11-2016

[53] Alibaba.com, Calcium Oxide,https://www.alibaba.com/trade/search?IndexArea=product_en&CatId=&fsb=y&floorTab=&SearchText=calcium+oxide, accessed on 7-11-2016

[54] Alibaba.com, Nitric acid,https://www.alibaba.com/trade/search?fsb=y&IndexArea=product_en&CatId=&SearchText=nitric+acid, accessed on 7-11-2016

[55] Alibaba.com, Sodium nitrate,https://www.alibaba.com/trade/search?fsb=y&IndexArea=product_en&CatId=&SearchText=Sodium+nitrate, accessed on 7-11-2016

[56] Alibaba.com,Sodium sulfate decahydrate,https://www.alibaba.com/trade/search?fsb=y&IndexArea=product_en&CatId=&SearchText=Sodium+sulfate+decahydrate, accessed on 7-11-2016

[57] P.Zhang, Z.W.Ma, "An overview of fundamental studies and applications of phase change material slurries to secondary loop refrigeration and air conditioning systmes", Renewable and Sustainable Energy Reviews, 16, 2012

[58] T.S. Evans, G.L. Quarini, "Investigation into the transporation and melting of thick ice slurries in pipes", International journal of Refrigeration, 31, 2008

[59] M.Randall, F.D. Rossini, "Heat capacities in aqueous salt solutions", The journal of the American chemical society, vol. 51, 1929

[60] D.E. Garrett, "Sodium Sulfate: Handbook of Deposits, Processing, Properties and Use", Academic Press, 2001

[61] National Institute of Standards and Technology, Water, http://webbook.nist.gov/cgi/cbook.cgi?ID=C7732185&Mask=1, accessed on 7-11-2016

[62] D. J. Rogers, G. J. Janz, Journal of Chemical & Engineering Data, 27 (1982) 424-428.

[63] The engineering toolbox, ice thermal properties, http://www.engineeringtoolbox.com/ice-thermal-properties-d_576.html, accessed on 7-11-2016